FABRICATION PROCESS AND CHARACTERISTICS OF A SILICON STRIP DETECTOR

by

DAVID J. MILLS

B.A.Sc., University of British Columbia, 1983

A THESIS SUBMITTED IN PARTIAL FULFILLMENT OF THE

REQUIREMENTS FOR THE DEGREE OF

MASTER OF Applied SCIENCE

in

THE FACULTY OF GRADUATE STUDIES

Department of Engineering Physics

We accept this thesis as conforming

to the required standard

THE UNIVERSITY OF BRITISH COLUMBIA

April 1985

22

In presenting this thesis in partial fulfilment of the requirements for an advanced degree at the University of British Columbia, I agree that the Library shall make it freely available for reference and study. I further agree that permission for extensive copying of this thesis for scholarly purposes may be granted by the head of my department or by his or her representatives. It is understood that copying or publication of this thesis for financial gain shall not be allowed without my written permission.

Department of Engineering Physics

The University of British Columbia
1956 Main Mall
Vancouver, Canada
V6T 1Y3

Date April 25, '85

ABSTRACT

The current and possible uses of semiconductor solid state detectors in nuclear physics are briefly discussed. The theory of solid state detectors is discussed with emphasis on the silicon PIN diode detector.

A fabrication process for silicon surface barrier position sensitive solid state detectors has been developed at UBC based on the work of J.B.A. England. A fabrication process recipe is included.

A prototype surface barrier detector system has been built and tested at UBC and TRIUMF using this process. The device has 1 mm position resolution in one direction, an active area of 40 mm in diameter and a mass thickness of 55 mg/cm^2. The measured efficiency for 50 MeV pions is 70% and expected rate capability is in excess if 1 MHz per strip. The detector efficiency is limited by a marginal signal-to-noise ratio.

TABLE OF CONTENTS

LIST OF TABLES

LIST OF FIGURES

ACKNOWLEDGEMENTS

I would like to express my thanks to Dr. L. Young for the use of the solid state laboratory in the Electrical Engineering department at UBC. I would also like to thank Dr. P. Janega and Dr. J.B.A. England for their technical advice in solid state fabrication techniques.

I am indebted to J. Creswell, D. Maas, G. Sheffer and P. A. Amaudruz for technical advice on electronics and nuclear experimental techniques. Many thanks to P. Amaudruz and the PISCAT group for time and help in the beam experiments.

Thanks are due to my supervisor Dr. Karl Erdman and to Dr. R.R. Johnson and Dr. D. Gill for encouragement and guidance during this project.

CHAPTER I

INTRODUCTION

The use of solid state detectors in nuclear physics is increasing. The development of fabrication technology has both reduced their cost and improved their quality.

What is a solid state detector?

The SS (solid state) detector is a slab of semiconducting crystal with an internal electric field generated by an external voltage applied across it. A charged particle or X-ray is detected when its passage through the crystal generates charge carriers which are swept out of the crystal by the internal electric field and are detected electronically as a current pulse (Figure 1.1).

SS detectors can be classified as either bulk or diode types. In bulk detectors the intrinsic conductivity of the semiconductor is very low due to high crystal purity or charge compensation techniques. One only needs to attach ohmic contacts to the normally insulating crystal to produce a detector.

The diode detector has less stringent restrictions on the bulk properties of the semiconducting material and uses the depletion zone created in a reverse biased pn junction as its active region. This active region can extend partially or

FIGURE 1.1

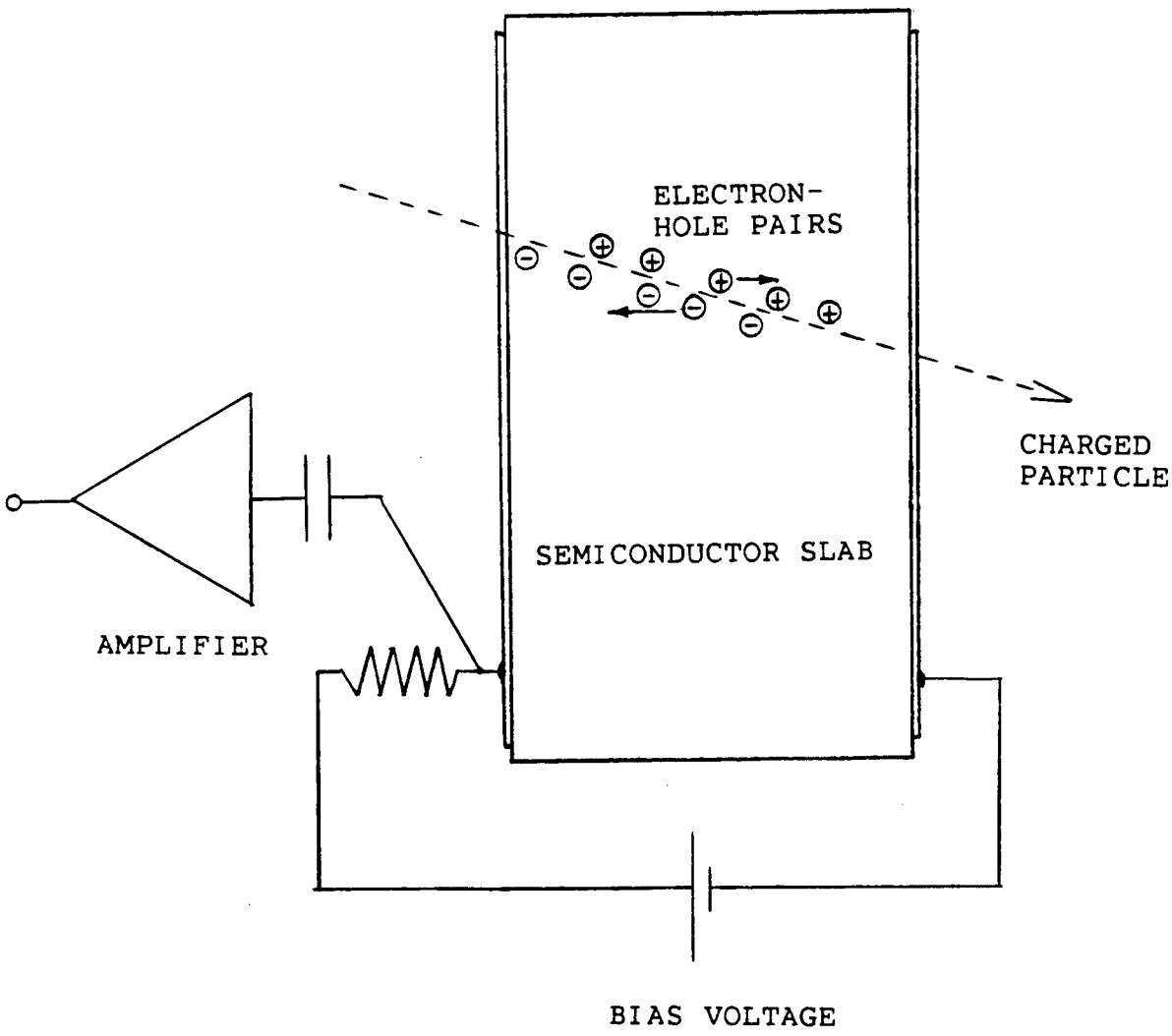

Schematic of a semiconductor charged particle detector.

completely through the crystal slab.

General properties of SS detectors

Solid state detectors can be designed for timing of particles, energy resolution, postition resolution or some combination of the three. The intrinsic properties of these detectors make them versatile devices with some unique properties.

SS detectors designed for small capacitance and high internal electric fields have pulse rise times in the order of nanoseconds with pulse widths of tens of nanoseconds. Accurate timing of events and high rate applications are thus possible.

Position resolution in SS detectors is achieved by patterning the charge collecting electrodes. With standard semiconductor photolithographic techniques, Si detectors have been built with 5 μm resolution for minimum ionizing particles (REF 6).

SS detectors can be used to determine the energy of stopped particles or the energy loss of transmitted particles. The charge pulse produced by the particle is directly proportional to the energy lost in the active region of the detector, and may be measured down to a few percent accuracy (REF 4). Historically, this has been the most common use for SS detectors. A single detector or stack of totally depleted detectors is commonly used to stop low energy particles or X-rays, and measure their energy.

The energy resolution or minimum energy detectable in a solid state detector is limited primarily by the random fluctuation of current flowing in the absence of particles. This leakage current depends on the integrity of the original semiconductor material and on the fabrication techniques used. Radiation damage can also contribute to leakage current, and the life of an SS detector is limited by the increase of the leakage current to some critical value. The most significant development in these detectors has been the reduction of leakage current to levels as low as 40 nA/cm^2 (REF 6).

These detectors are typically less than 5 cm in diameter and greater than 100 μm thick ($\simeq$25 mg/cm^2). This relatively small area and large mass thickness is less of a drawback when one considers that other position sensitive or timing detectors require bulky light pipes and photomultipliers or gas containment systems. At present, position sensitive solid state detectors need large arrays of preamplifiers, but in future even this may be avoided with amplifiers or CCD readouts being built on the same semiconductor wafer as the detector. At present SS detectors are used extensively in low energy physics due to their good behavior in high vacuum.

Motivation for detector development at TRIUMF

The high rate capability of position sensitive SS detectors was the primary motivation for building them at TRIUMF. The TRIUMF M13 pion beamline can have pi^+ fluxes in excess of $2x10^6$/s. A high rate detector can be used in this

FIGURE 1.2

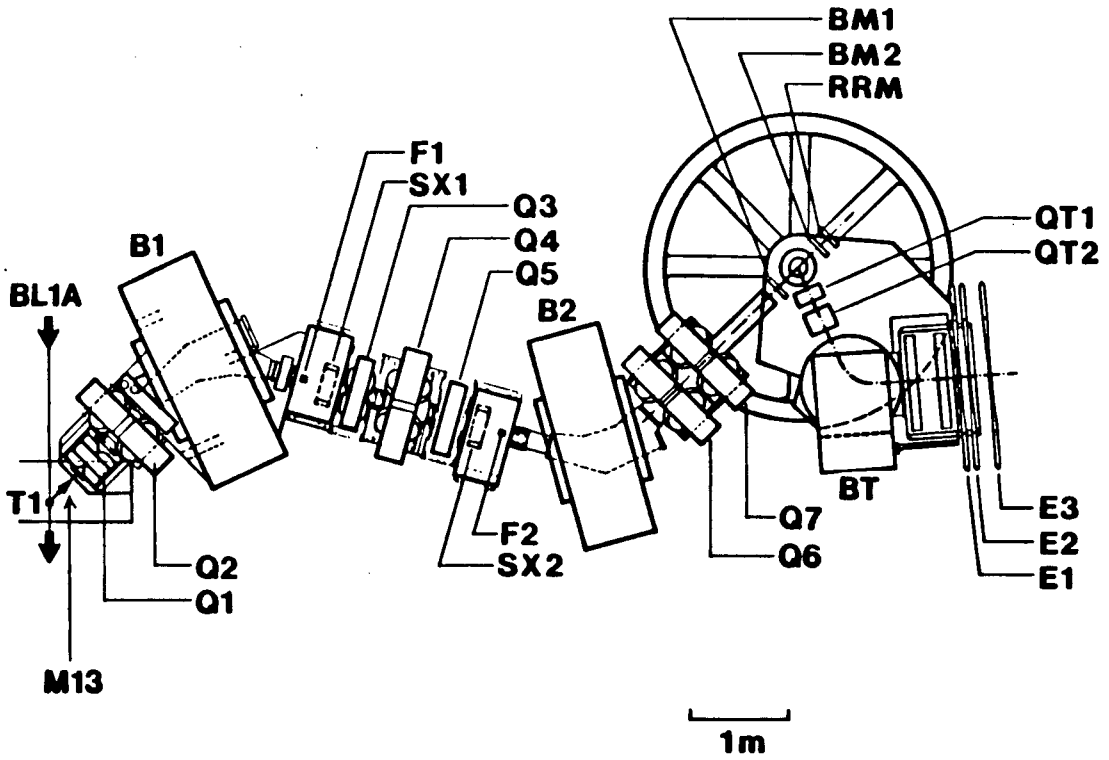

M13 pion beam line at TRIUMF. B1 and B2 are dipole bending magnets; F1 and F2 are the focus locations of the momentum selection slits.

channel as a beam profile monitor for diagnostics or as a tool in scattering experiments. Currently the momentum resolution of the pion beam is selected by a pair of slits located at focuses downstream of a bending magnet (F1, F2 in Figure 1.2). A SS detector located at one of these focuses can be used to tag the position and therefore the momentum of each particle as it traverses the channel. The slits can then be opened to increase the pion flux without degrading the momentum resolution. In a similar manner, a solid state detector at the scattering target can be used as a position monitor to improve the energy resolution of the spectrometer.

A position sensitive, silicon, solid state detector has been built and tested by the PISCAT (pion scattering) experimental group at TRIUMF. The device was made using silicon surface barrier techniques. It has a resolution of one millimeter in one direction and an active area of 4 cm in diameter and is 230 μm thick (55 mg/cm^2),(Figure 1.3).

FIGURE 1.3

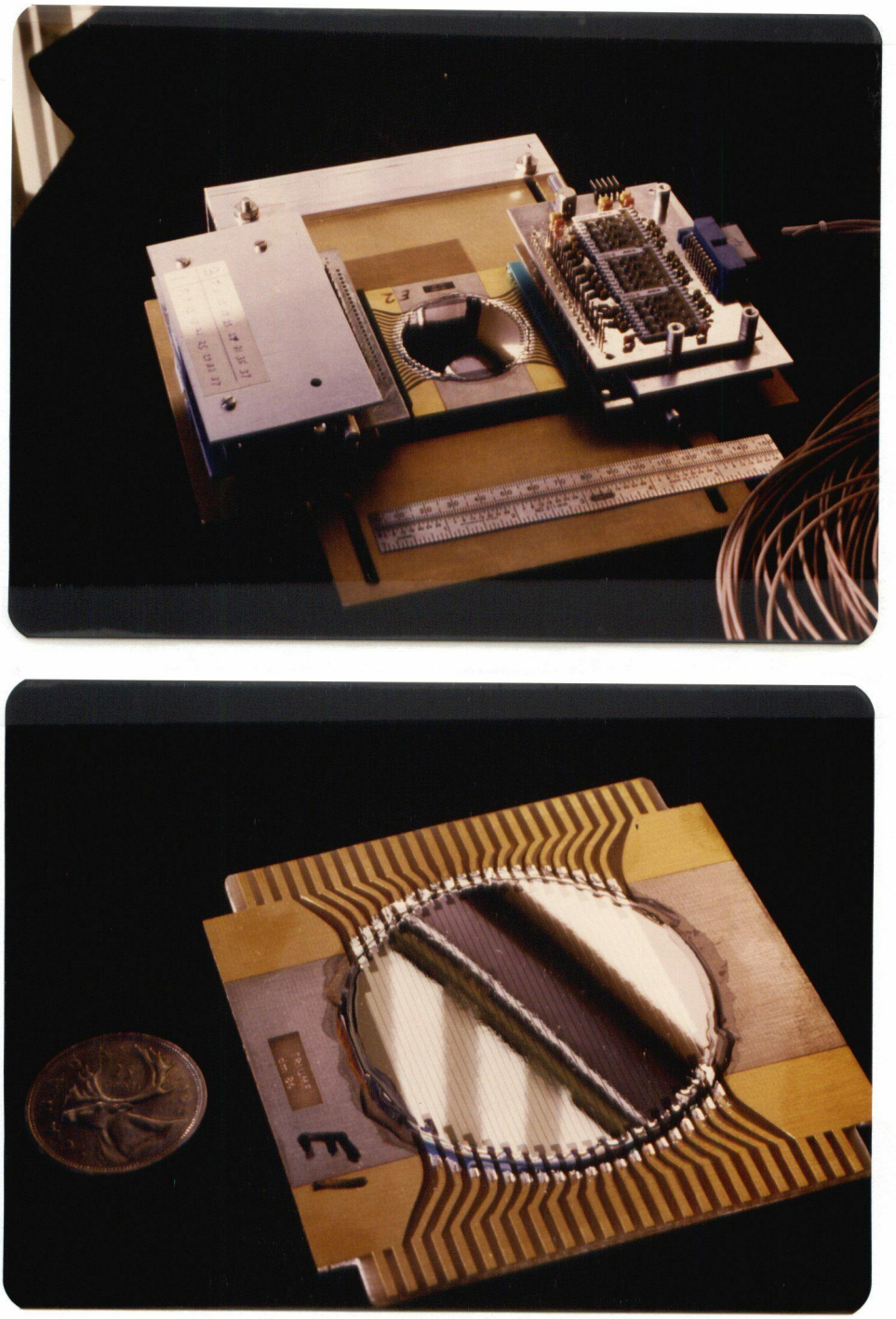

Surface barrier, position sensitive, solid state detector manufactured at UBC. The pre-amplifier readout electronics are visible.

CHAPTER II

PRINCIPLES OF OPERATION

Basic band theory of semiconductors and charge generation

A semiconductor is a crystal with a gap in the available energy states for electrons. The states above the gap are normally empty and are collectively known as the conduction band. Similarly, the valence band is the collection of normally full states below the band gap. In any crystal at zero temperature electrons are lying in the lowest energy states possible without violating the Pauli exclusion principle. At zero temperature the Fermi energy is defined as the energy above which no electrons are seen. At non-zero temperatures, the Fermi energy, E_F, defines the thermal distribution of electrons or holes (REF 8):

$$n = N_C e^{-(E_C - E_F/kT)}$$

$$p = N_v e^{-(E_F - E_V/KT)}$$

Equations 2.1

where n and p are the respective densities of electrons and holes, E_C is the electron energy in the conduction band, E_V is the hole energy in the valence band, N_C and N_v are densities of states for the conduction and valence bands respectively

and kT is the temperature in energy units. Holes are electron vacancies in the almost full valence band and behave like positive charged particles with a mass close to the mass of the electron (effective mass). Both electrons and holes have an effective mass in the crystal which depends on the state occupied by the particle and on its direction of motion in the crystal lattice. Effective masses of charge carriers in semiconductors usually are between 10% and 100% of the electron mass and holes can be "heavier" or "lighter" than electrons. Intrinsic semiconductors are characterized by the Fermi energy lying close to the centre of the band gap. Insulators are the same but with a larger band gap.

In a solid state detector the active volume of semiconducting crystal normally acts like an insulator. The non-conducting state has an empty conduction band (no electron charge carriers) and a full valence band (no hole charge carriers). When a charged particle passes through the crystal it scatters electrons into the available energy states in the conduction band, leaving behind empty sites (holes) in the valence band. This excited configuration quickly decays by phonon excitation, radiative decay or scattering from valence electrons (generating more electron-hole pairs) until a quasi-stable state is reached (10^{-12}s). This longer lived state is characterized by an equal number of electrons and holes in the conduction and valence bands. These charge carriers are free to drift in the internal electric field of the detector and form the detected current pulse (Figure 2.1).

FIGURE 2.1

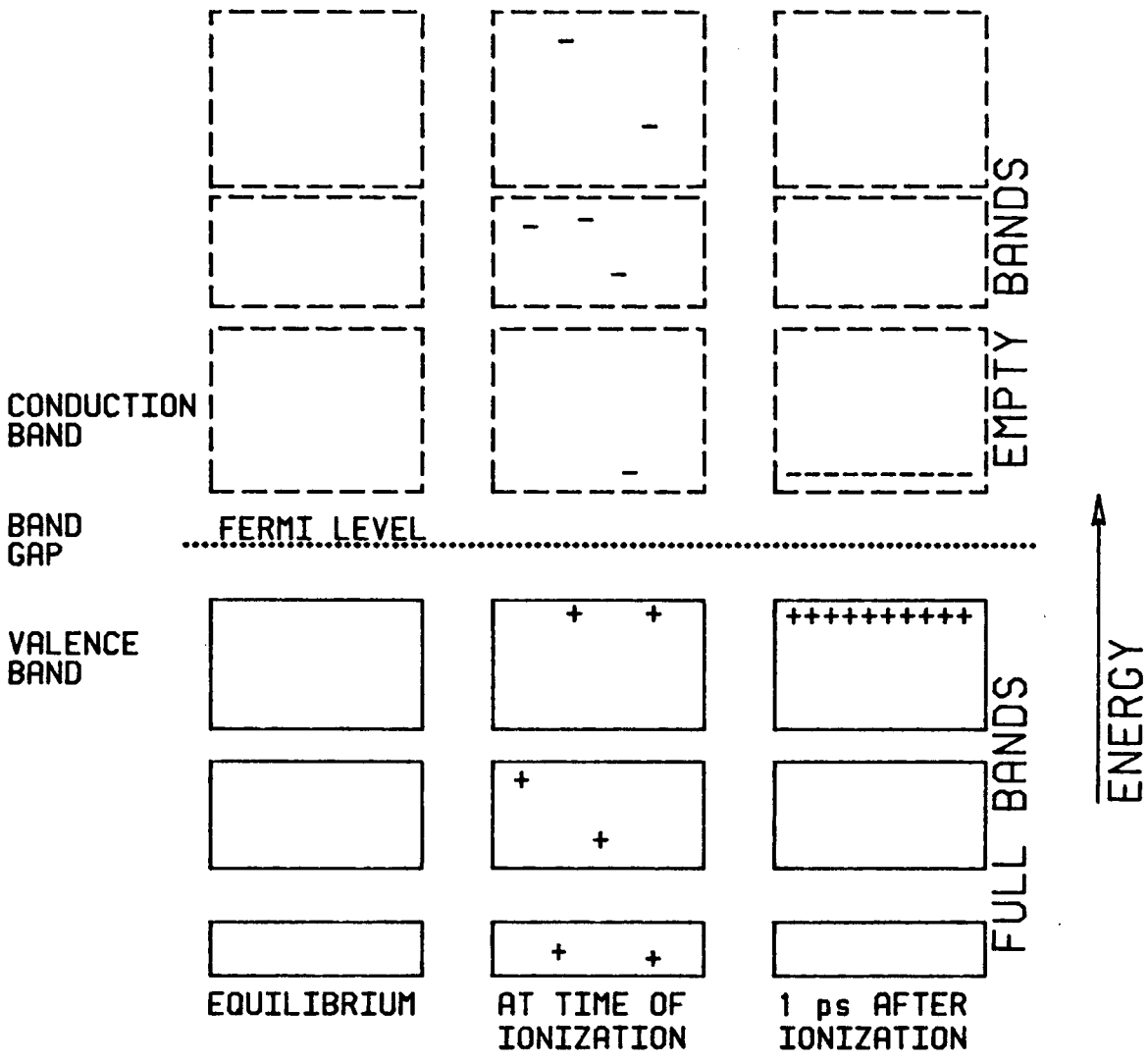

Schematic of charge generation process in the active region of a solid state detector.

The size of this current pulse, Q, is proportional to the energy loss, ΔE, of the detected particle in the active region and is given by

$$Q = qK\Delta E/E_{gap}$$

Equation 2.2

where Q is the charge generated in the detector (either holes or electrons), E_{gap} is the band gap of the semiconductor (1.12 eV for Si) and q is the electronic charge. K is a factor less than one that accounts for energy losses other than ionization, for example phonon excitation. K is about 1/3 in Si as 3.2 eV is the average energy required to produce an electron hole pair (REF 7). Gas ionization chambers require about 30 eV per ionization and often use avalanche charge multiplication near collection wires. Avalanche charge multiplication also occurs in semiconductors with a high internal electric field. This effect is not easily controlled, however, and often causes total breakdown, so it is not used in semiconductor charged particle detectors.

Bulk type SS detectors, resistivity of semiconductors

Bulk SS detectors are made from high resistivity semiconductor. An external voltage, V, applied to contact electrodes generates an internal electric field in the detector slab. For a slab of thickness d, the electric field strength is uniformly V/d.

One limitation of bulk detectors is the finite resistivity of the crystal due to thermally excited charge carriers. The leakage current of bulk detectors can be calculated from semiconductor properties. In thermal equilibrium the carrier concentration is given by Equations 2.1 or

$$np = n_i^2 \simeq e^{-E_{gap}/kT}$$

Equation 2.3

where n and p are the density of electrons and holes respectively, n_i is the intrinsic carrier concentration, E_{gap} is the semiconductor band gap, kT is the absolute temperature in energy units. A proportionality constant dependent on density of states is omitted. The intrinsic carrier concentration is shown in (Figure 2.2) for Ge, Si, GaAs. The electron leakage current per unit area, J_n, in an ideal bulk detector ($n=p=n_i$) is (REF 8):

$$J_n = qn_iE\mu$$

Equation 2.4

where q is the electric charge, n_i=n is the electron carrier concentration, E is the internal electric field and μ is the electron mobility. For example, at room temperature with a 1kV/cm electric field, the best leakage currents for Ge, Si, GaAs bulk detectors are 14 A/cm^2, 3 mA/cm^2 and 2 μA/cm^2 respectively. Of these three only GaAs has an acceptable behavior at room temperature.

FIGURE 2.2

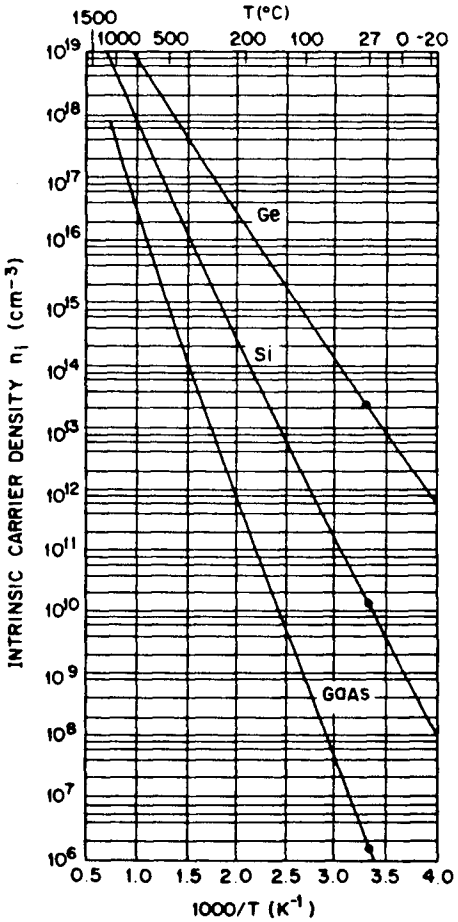

Intrinsic charge carrier concentration of Ge, Si, and GaAs as a function of inverse temperature (after Sze Ref. 8).

In a non-ideal bulk detector, leakage current can be produced by the injection of charges into the crystal by the contact electrodes if special care is not taken to make the contacts ohmic. Unwanted donor or acceptor impurities can contribute charge carriers as can mid-band generation and recombination sites caused by impurities or crystal faults. Further discussion of leakage current is included in the section on diode detectors. Recent improvements in the quality of commercially available semiconductors are making bulk detectors more feasable. Bulk detectors made from large band gap semiconductors such as GaAs or GdS may be common in the future.

Diode detectors' electrical characteristics

In diode type SS detectors, it is the depletion zone of a reverse biased pn junction that provides the semi-insulating active volume for charged particle detection. The electrical properties of all junction SS detectors are approximated by the PIN diode (Figure 2.3). The $p^+n^-n^+$ diode will be considered here although the $p^+p^-n^+$ is similar.

Let us consider the interface of the highly doped p^+ region and the lightly doped n^- region. This pn junction can be made by diffusing or implanting a class III dopant element such as boron into an n^- substrate or by the construction of a surface barrier. In a p type doped semiconductor, there are fewer electrons per lattice site than in intrinsic material

FIGURE 2.3

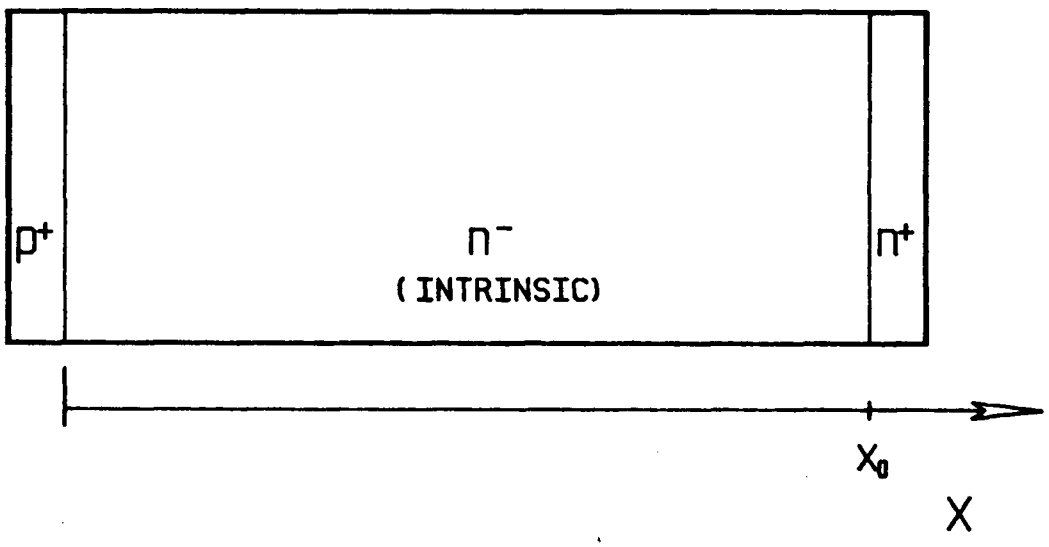

Schematic of PIN diode and definition of coordinate x.

FIGURE 2.4a

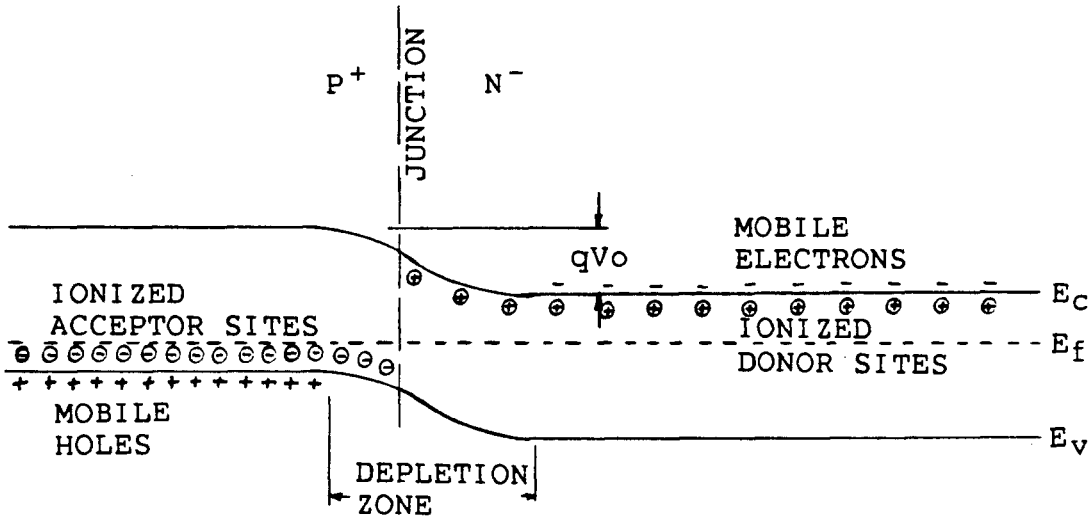

FIGURE 2.4b

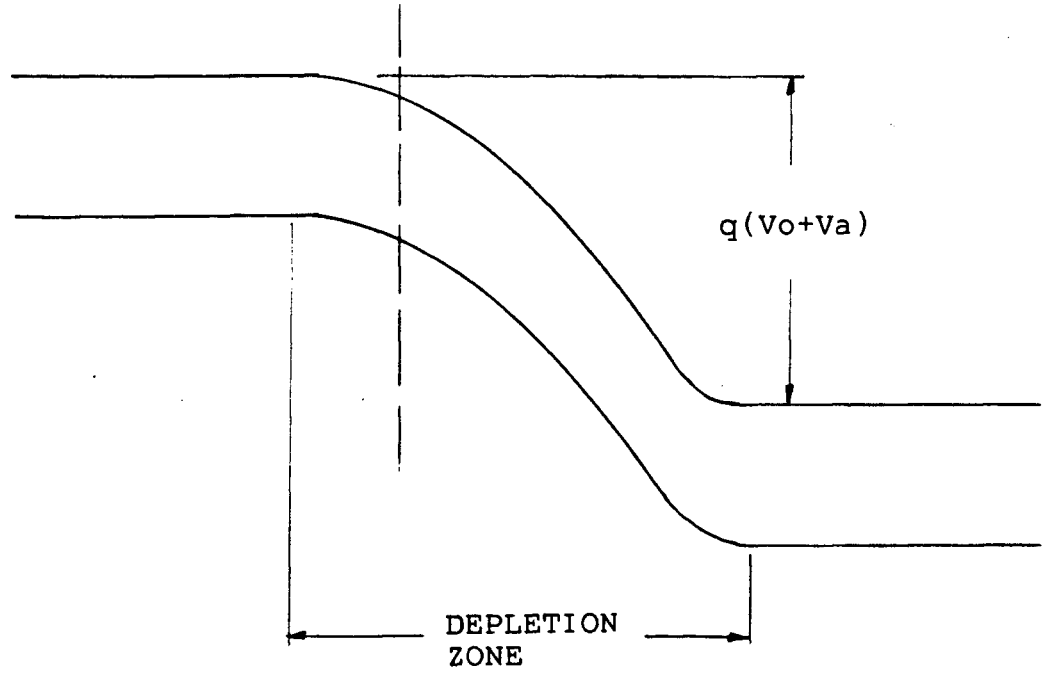

Band diagrams for pn junction with (a) no external applied voltage, (b) an applied voltage of V_a. E_c and E_v are the energies of the bottom of the conduction band and the top of the valence band respectively; E_f is the Fermi energy and q is the electronic charge.

and the Fermi level is consequently shifted downward in energy toward the bottom of the band gap. Similarly the Fermi level is shifted upward toward the top of the band gap in an n type semiconductor.

In the absence of any external field, there is a redistribution of charges such that the Fermi level is constant throughout the crystal. This leaves a region depleted of free charge carriers near the junction. The energy levels of the valence and conduction bands are a function of the local charge distribution and thus change across the pn junction (Figure 2.4). In equilibrium the depletion zone barrier is precisely large enough to prevent diffusion of holes into the n region or electrons into the p region in the large concentration gradients.

When an external voltage V_a is applied across the junction with the same sign as V_0 (reverse bias), free charges move away from the junction and leave a larger depletion zone; the barrier height increases proportionately (Figure 2.4). In a totally depleted PIN diode, the depletion zone extends across the crystal to the n^+ region. In the approximation that the n^- or intrinsic region of the diode has a much lower dopant density than either the p^+ or n^+ regions and assuming that the depletion zone is totally depleted of charge carriers, one can calculate the depletion width and internal electric field shape as a function of applied voltage V_a (REF 7, Figure 2.5).

FIGURE 2.5

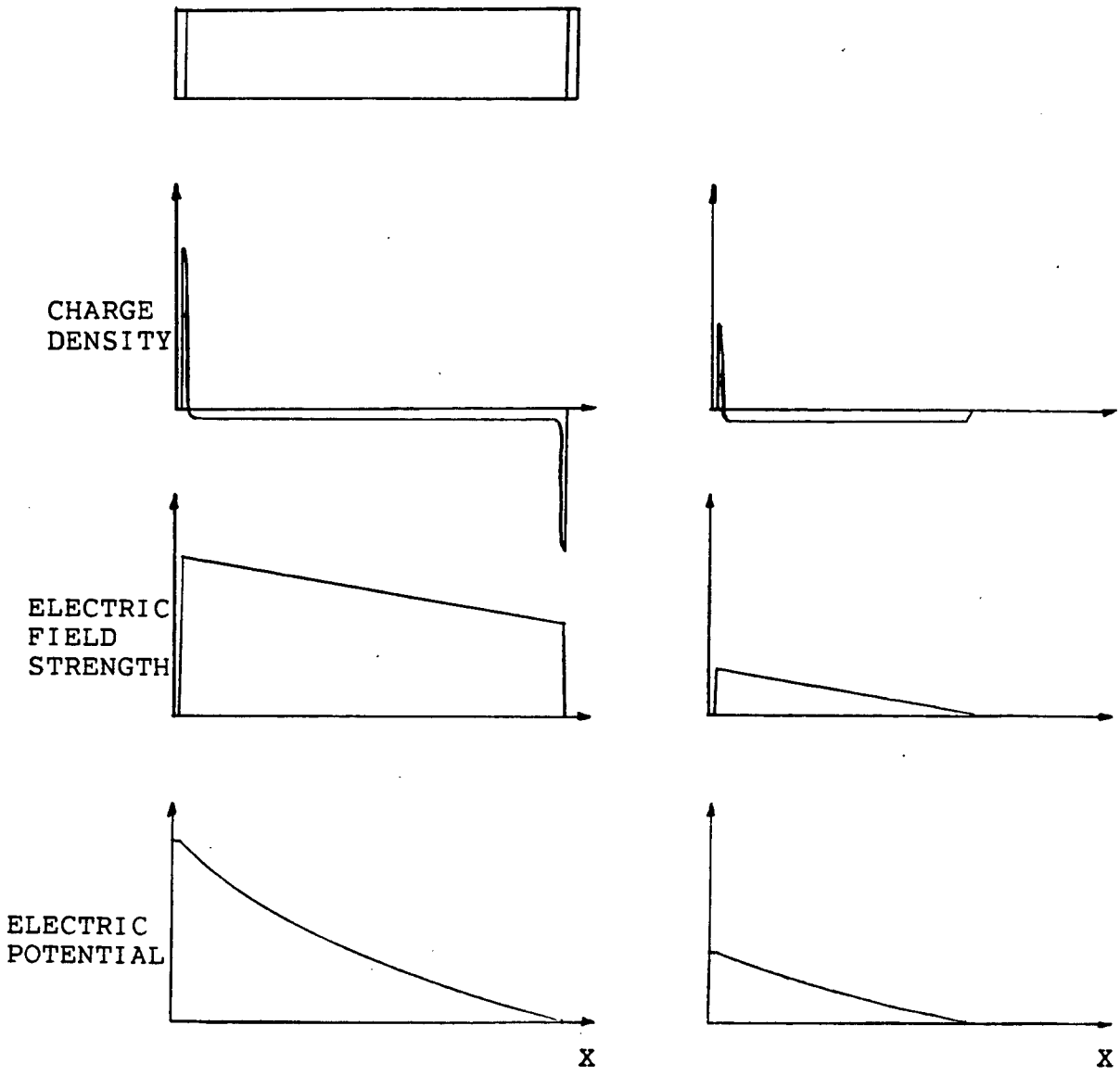

Qualitative charge density, electric field and potential as a function of position in a reverse biased PIN diode. Charge density is proportional to the concentration of uncompensated ionized dopant ions.

For an SS detector that is not fully depleted, the depletion width, W, is given by (REF 7)

$$W^2 = 2(V_o+V_a)\epsilon_s/q\rho_n$$

Equation 2.5

where V_o is the built in depletion potential with no applied voltage, V_a is the applied voltage, ϵ_s is the dielectric constant of the semiconductor, ρ_n is the density of dopant ions in the n^- region and q is the electronic charge. The electric field is calculated by integrating the charge density in the depletion zone and is thus linear (REF 8):

$$E(x) = (W-x)\rho_n/\epsilon_s \qquad 0 < x < W$$

$$= 0 \qquad \text{elsewhere}$$

Equations 2.5

where x is defined in Figure 2.3.

For a totally depleted diode the depletion width is fixed at the width, x_o, of the intrinsic region. The electric field is still linear with the same slope as in a partially depleted diode, but now has maximum and minimum values (E_{max}, E_{min}) dependent on the applied voltage (Figure 2.5).

$$\Delta E = E_{max} - E_{min} = q\rho_n x_o/\epsilon_s$$

$$E(x) = (x_o - x)\Delta E/x_o + E_{min} \quad 0<x<x_o$$

$$= 0 \qquad \text{elsewhere}$$

$$V_a + V_o = x_o(E_{min} + \Delta E/2)$$

Equations 2.7

The electric potential at any point in the crystal is found by integrating the electric field. The potential difference across the whole crystal is the applied voltage, V_a, plus the built-in potential, V_o (Figure 2.5). Totally depleted PIN diodes are convenient detectors because the depletion width (active region) and capacitance are constants. The high frequency capacitance, C, of the PIN diode with depletion width W is the same as a parallel plate capacitor of the same width (REF 8)

$$C = A\epsilon_s/W$$

Equation 2.8

where A is the area of the diode.

Charge collection time

The signal response time in a SS detector is dependent on the drift time of charge carriers and on the RC time constant of the detector/preamplifier system.

The drift velocity, v, of charge carriers in a semiconductor is proportional to the electric field, E, in the crystal (REF 8).

$$v = \mu E$$

Equation 2.9

(REF 8) where μ is the carrier mobility. The mobility for electrons is higher than that for holes and varies with temperature, doping concentration and semiconductor type. Carrier mobilities for lightly doped semiconductors at 300 K are shown in Table 2.1 for Ge, Si and GaAs.

Table 2.1 Carrier mobilities at 300 k (cm^2/Vs)

	Ge	Si	GaAs
Holes	1900	450	400
Electrons	3900	1500	8500

It should also be noted that the drift velocities in these three semiconductors start to saturate above fields of 3000 V/cm at a value near 10^7 cm/s (REF 8). For a fully depleted SS detector of thickness d, the longest drift time is given by:

$$t = \int_0^d dx/V(x) = \int_0^d dx/\mu E(x)$$

$$= (d/\mu\Delta E)\ln(E_{max}/E_{min})$$

Equation 2.10a

where E_{max}, E_{min}, ΔE are defined in Equations 2.7. For a partially depleted detector E_{min} is zero but, as the electric field is linear, 90% of the charge is collected in

$$t_{90} = (.9W/\mu E_{max})\ln(10)$$

Equation 2.10b

where W is the depletion width. In a bulk detector the collection time is

$$t = d/\mu E$$

Equation 2.10c

where E is V/d, the uniform electric field. For a hypothetical 200 micron Si detector similar to the one built at TRIUMF, the collection time would be

$$t = t_o \ln(E_{max}/E_{(min)})$$

Equation 2.10d

where t_o = 4 ns for electrons and t_o = 13 ns for the slower holes. The capacitance for such a detector is about 50 pF/cm². This detector made with small area strips, fast electronics and operated with a large bias voltage will have pulse rise times on the order of nano-seconds and pulse separation down

to 30 ns , depending on electronics response time.

The efficiency for charge collection in SS detectors is very high as the carrier lifetime is long in the depletion zone. Carrier lifetimes are on the order of milliseconds in high resistivity silicon at room temperature. GaAs has shorter carrier lifetimes ($\simeq$10 μs) due to allowed radiative electron hole recombination, but lifetimes in the depletion zone are still long compared to collection time.

Energy resolution, noise, leakage current

It has already been stated that a charge collected by a SS detector is proportional to the energy deposited in the active region of the device. The energy resolution, or the minimum energy detectable, is limited by the noise in the system. Noise in SS detectors is due to the variation in charge generated by a mono-energetic particle and the background noise intrinsic to the detector/amplifier system.

The distribution in the amount of charge generated by a stopped mono-energetic particle has a statistical variance associated with it dependent on the average energy, ξ, required to produce an electron-hole pair. The width of the ideal pulse in terms of energy is (REF 7):

$$W = 2.96(\xi E)^{1/2}$$

Equation 2.11

where E is the energy of the incident particle. Because of the small size of ξ (3.2 eV for Si) this uncertainty due to statistics is negligible for SS detectors. The statistical error in measuring a 6 MeV alpha particle with a Si detector is only 11 KeV (REF 7). Gas proportional chambers or scintillators have a larger effective energy per detected electron (30 eV to 500 eV), and consequently have larger statistical errors in energy resolution.

The intrinsic noise in a reverse biased junction is due mostly to shot noise and thermal noise.

Shot noise, due to finite carrier charge, is directly proportional to leakage current, I_s. The mean square shot noise current is (REF 8)

$$\langle i_n^2 \rangle = 2qBI_s$$

Equation 2.12

where B is the frequency bandwidth of interest.

Thermal noise is proportional to temperature and to the conductance, G, of the device (REF 8):

$$\langle i_n^2 \rangle = 4kTBG$$

Equation 2.13

Both these noise mechanisms have a uniform or white frequency

spectrum and are therefore limited by the bandwidth of interest. A third source of noise, flicker noise, is not important in the high frequency band of interest for SS detectors due to its 1/f frequency spectrum.

For a given leakage current I_s, the noise expected is (REF 8)

$$\langle i_n^2 \rangle = 2qBI_s \ (1+e^{qV/KT})$$

Equation 2.14

where q is the electronic charge, B is the bandwidth of interest, V is the bias voltage and kT is the temperature energy. The second (thermal) term has been simplified using the Shockly diode equation to calculate conductance. Empirically, one can detect a current pulse approximately one tenth of the magnitude of the leakage current.

The leakage current is partially described by the theoretical diffusion current (first term, Equation 2.15) and generation current (second term, equation 2.15) in a pn step junction diode:

$$J_R = I_s/A = q\sqrt{D_p/\tau_p}(n_i^2/N_D) + qn_iW/\tau_e$$

Equation 2.15

where D_p is the diffusion constant for holes, τ_p and τ_e are the respective hole and electron lifetimes, n_i is the intrinsic carrier concentration, N_D is the donor concentration in the n region, and W is the depletion width. Recall that the

intrinsic carrier concentration increases with temperature (Equation 2.3) while lifetime decreases; the leakage current thus has a strong temperature dependence. The lifetime for carriers is also reduced by impurities (generation and recombination sites) in the crystal and by lattice faults. Further contributions to leakage current come from injection of carriers from the back contact in a totally depleted detector as well as resistive leakage at the edges of the device. In surface barrier detectors, voltage dependent Schottky emission contributes to the leakage current and surface states often dominate generation current in the depletion zone. Leakage current in room temperature SS detectors is the primary engineering problem due to the large surface area and depletion depth required for useful devices.

Leakage current, radiation damage

Radiation contributes to leakage current and noise by causing lattice faults and by isotope production. In the absence of slow neutrons, it is the former mechanism which dominates radiation damage. Lattice damage causes charge traps which slow detection response times, reduce charge efficiency, and increase leakage current. Heavy ions deposit more energy in a detector and do proportionately more damage. Crystal lattice damage can sometimes be annealed out by low temperature (less than 400°C) heat treatment in implanted or diffused devices. Ion implanted detectors have been shown to have a lifetime of 10^{11}-10^{14} particles/cm² in a muon flux (REF

9). Surface barrier detectors tend to have shorter life expectancies.

In a slow neutron flux ^{30}Si (3% abundant) can absorb a neutron and subsequentally β decay to phosphorus. Phosphorus is a donor dopant and will make the crystal more n type. In addition, decay of radio-isotopes in the detector active region will add noise signals.

Depletion depth, energy resolution

To measure the energy of stopped particles in an SS detector, it is necessary that the particle stop in the active depletion zone. A stack of totally depleted SS detectors can have more than 99% of their volume depleted and are ideal for measuring the energy of medium to low energy particles or X-rays. To measure low energy particles, a single solid state detector with an appropriately large depletion depth is used. The low energy limit of resolution is reached when the range of the particle of interest approaches the thickness of the dead zone at the surface of the detector. This dead zone is characterized by the thickness of the metal contacts on the surface and the distance to the edge of the depletion zone. The dead zone can be reduced to hundreds of Angstroms in surface barrier detectors. The absolute thickness of the dead zone can be estimated by measuring the energy of a detected particle as a function of the angle of incidence for a collimated monoenergetic source.

Transmission detectors

SS detectors are often used to detect particles by their energy loss in transmission. Assuming that the energy loss is small compared to the total energy of the particles, the detected pulse is proportional to the depletion depth. As it is normally desireable to reduce scattering, fully depleted thin detectors are used. When measuring the energy loss of a transmitted particle, one is also measuring the substantial energy straggle (≃20% of energy loss). Even with such a large built-in uncertainty, energy resolution is used to distinguish particles with different rates of energy loss in matter. The primary problem in a transmission detector is to detect the small signals associated with thin detectors and particles with low energy loss.

The signal-to-noise ratio of totally depleted detectors can often be improved by increasing the bias voltage across the device. According to Equations 2.7 and 2.10, this speeds up the charge collection, increasing the height of the current pulses. However, in a totally depleted detector with a large applied bias voltage, injection current at the back contact can become a problem as can breakdown effects. The breakdown voltages of implanted or diffused PIN diodes are larger than surface barrier devices and all types behave better with very high resistivity intrinsic regions. Breakdown occurs if the internal electric field exceeds a critical value (somewhat higher than 10^5 V/cm) or if the depletion zone moves through

the back contact (or front contact in surface barrier devices). These processes are called avalanche breakdown and punchthrough respectively.

Minimum ionizing particles can be detected in room temperature SS detectors as thin as 100 microns if care is taken to reduce noise. This corresponds to a signal of around 10^4 electrons.

It should be emphasized that the signal to noise behavior of any SS detector is intimately related to the readout electronics. It is the behavior of the detector/electronics system that should be optimized for any given application.

Position resolution

Position sensitive detectors are made by patterning the charge collecting electrodes on the surface of the detector. Photolithographic techniques developed for the electronics industry can reproduce features with one micron dimensions. Less exacting techniques have been used by Kemmer et al to produce SS strip detectors with 5 micron resolution in one direction (REF 6). This high resolution was accomplished using 20 μm strip spacing, an amplifier on every third strip and charge interpolation between readout amplifiers. The theoretical limit on position resolution in SS detectors may be the width of ionization tracks in SS detectors or the diffusion length, L, of carriers before they are collected. (REF 8)

$$L = (Dt)^{1/2}$$

Equation 2.16a

where D is the diffusion constant for charge carriers and t is the time of interest. The diffusion constant is related to carrier mobility μ and temperature (REF 8):

$$D \simeq \mu kT/q$$

Equation 2.16b

Electrons in silicon will diffuse an average of 6 μm in 10 ns at room temperature. Detectors made with CCD readouts or integrated preamplifiers could make large area high resolution two dimensional detectors more feasable by reducing the density of electronics required for a high resolution small area detector.

In all types of detectors it is important to protect (passivate) the surface of the semiconductor from impurities in the environment (REF 8). In a position sensitive SS detector the surface should be passivated between electrode strips. Two examples of surface passivation techniques are used in the two processes described in Chapter III.

CHAPTER III

FABRICATION OF DEVICES

With a recognized need for SS detectors at TRIUMF, it was decided that position sensitive silicon devices should be fabricated at UBC. Position sensitive devices are available commercially but they are still very expensive. The fabrication work was done primarily in the Electrical Engineering Solid State Laboratory. The main thrust of the work was to reproduce the ion implantation techniques used by Kemmer et al (REF 6) and the surface barrier techniques used by England (REF 3,5,12). England's surface barrier technique proved to be simpler and more successful, and will therefore be emphasized in this discussion.

Ion implanted SS detectors

The implanted detector developed by Kemmer (REF 6) in 1980 is a standard PIN diode as described in Chapter II, but made in a pattern of strips so as to be position sensitive. A fabrication flow chart is shown in Figure 3.1. This type of detector is attractive because of its very low leakage current (Kemmer claims 40 nA/cm^2), even when biased well above the total depletion voltage. Also desireable is the quality of the surface passivation that makes the detector almost immune to environmental contamination after fabrication. It was not possible to make a low leakage SS detector using this

FIGURE 3.1

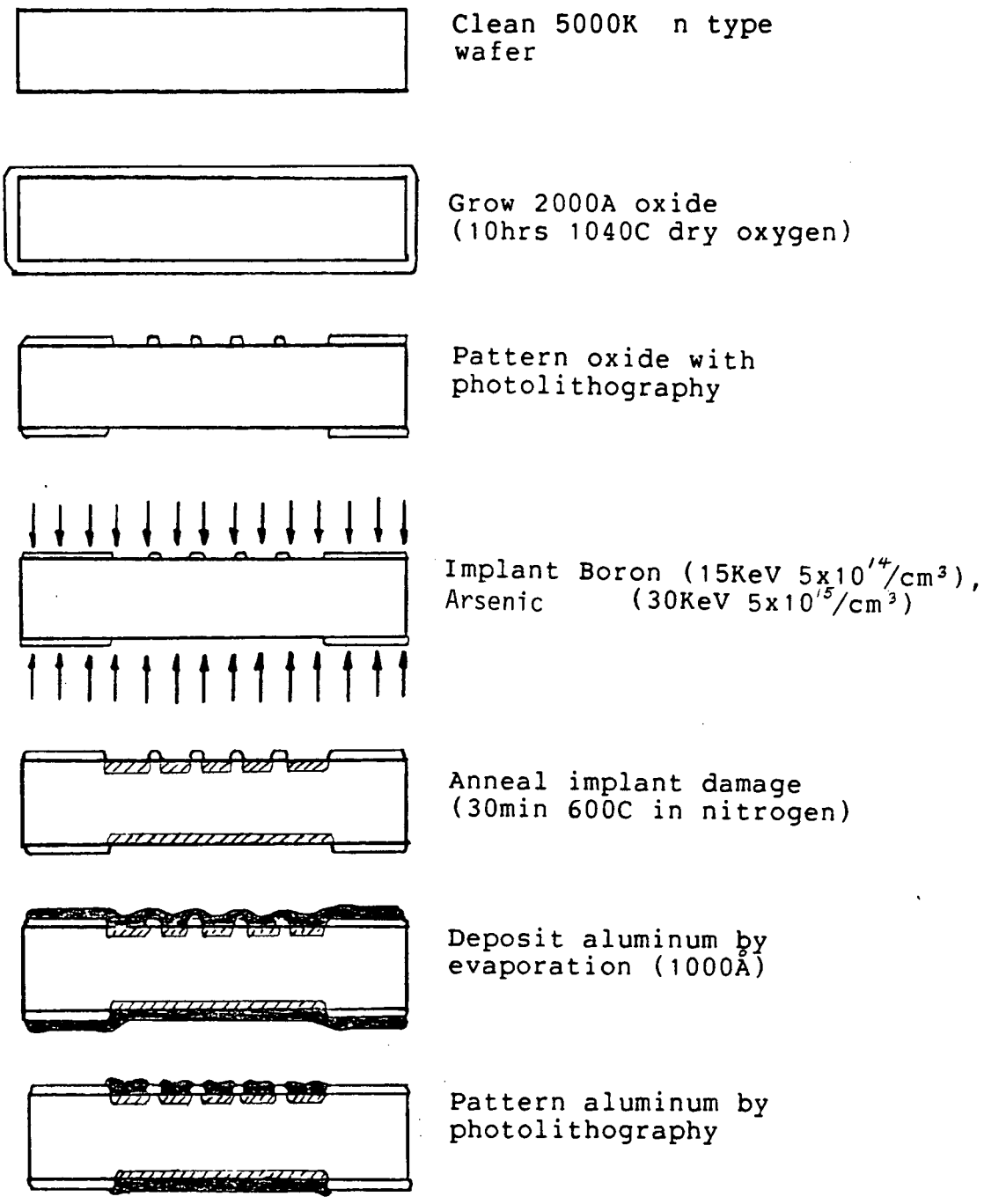

Kemmer's implanted detector fabrication process. Note that the silicon surface is protected from the environment by either aluminum or silicon-oxide (Ref. 6).

technique in the development time available. The best detector built using a modified process had a leakage of 10 $\mu A/cm^2$ and was not uniform from strip to strip.

The most common problem in any solid state fabrication is cleanliness. The large number of steps in this process make contamination of the wafer more likely if a highly controlled clean environment is not available for the fabrication process. The E.E. laboratory at UBC lacked this quality of cleanliness in both dry and wet processing steps. In an environment like the E.E. laboratory that is not completely controlled. Wet steps like photolithography can introduce impurities to the surface of the detector wafer and high temperature steps like oxidation and annealing can drive impurities into the bulk regions of the detector.

The integrity of the crystal lattice is also dependent on its temperature history. High temperature treatment can lower the resistivity of the semiconductor even in a clean environment.

Since ion implantation doping also damages the surface of the crystal this damage must be annealed out at high temperatures. The temperature as a function of time used in the anneal process is very important. During the anneal process dopant ions diffuse and are incorporated into the crystal lattice. At the same time, the crystal faults heal themselves or move towards the surface. The amount of annealing necessary is dependent upon the energy and dose of

the implanted dopant atoms and upon the desired dopant "activation" (the percentage of dopant incorporated into the crystal lattice, the rest remaining interstitial). Kemmer recommends annealing at 600°C for 30 minutes, but the best results at UBC were achieved with an 800°C anneal for 16 hours (REF 14). Others recommend high temperature short anneal processes (REF 13). The anneal process certainly affects the leakage current of implanted detectors, and further experimentation is required to optimize this process at UBC. An option that may be considered in the future is surface annealing with high power arc lamps.

The Kemmer process will probably have to be modified before consistent results can be achieved in a laboratory without extensive environmental control. For example, lower temperature sputtering or plasma techniques could be used to deposit the mask/passivation oxide. A surface etch before oxidation may prove to be better than the RCA cleaning technique used at UBC. Generally speaking, it is not always possible to transplant a fabrication process from one laboratory to another without carrying out a time-consuming redevelopment procedure.

Surface barrier SS detectors

A surface barrier fabrication process was developed more than ten years ago at the University of Birmingham by J.B.A. England (REF 10). His detector is an n^- wafer with a Si/Si-oxide/Ge tunnel diode on both surfaces (Figure 3.2).

FIGURE 3.2

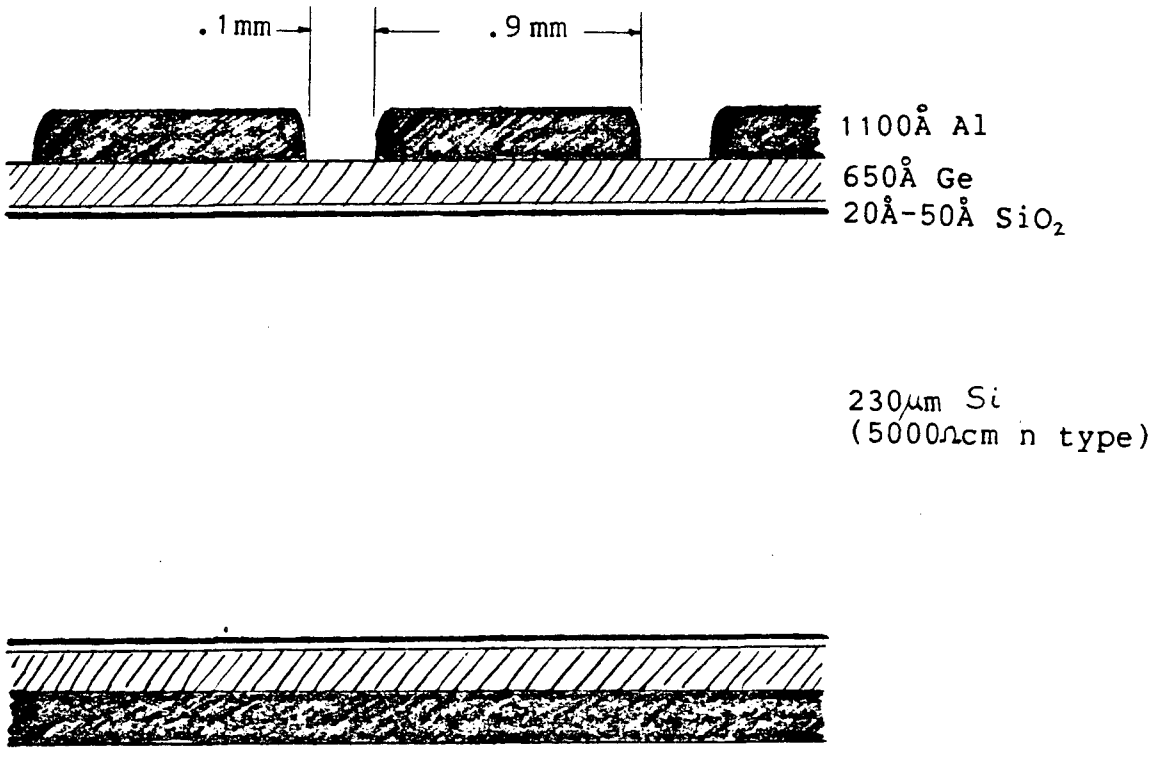

Cross section of the surface barrier strip detector built at UBC (modified England technique, Ref. 3,5,10,12). Front and back are identical except for patterns in aluminum.

Surface electrodes of Al or Au are used to reduce the sheet resistance of the device and to provide a pattern for position sensitive detectors. The fabrication process is short, requiring only one day in the laboratory. This reduces the probability of contamination or other mistakes during manufacture. The detector crystal is never heated above 100°C in the England process and thus its bulk properties are not degraded. Surface barrier SS detectors do have shorter lives in radiation and, in theory, a higher leakage current than a similar implanted device. The low cost and simple process for fabrication of surface barrier devices may make these problems unimportant.

The recipe detailed in Appendix A is the best of several attempts at duplicating England's process, and is only slightly modified from his recommendations (REF 12). Two low leakage detector wafers were fabricated using this process with aluminum metalization. Several parts of the process proved to be quite important.

As previously mentioned, cleanliness is of primary importance. It was found that wafers that were not etched produced diodes with large leakage currents, even if they were carefully cleaned. England also claims that deionized filtered water is not clean enough for the process and recommends only distilled, filtered, deionized water. Similarly, utensils and chemicals must be very clean and pure. Only after the edges are protected by epoxy and the surface is protected by

germanium is the detector relatively safe from contamination of the surface. The germanium provides excellent surface passivation due to its gettering effects (ability to trap impurities); this is one of the attractive properties of the England surface barrier detector.

Etching of the silicon surface provides an ideal opportunity to choose the thickness of the final device. However, it was found that even with continuous agitation of the etch bath and careful quick quenching of the etch, the Si surface was left mottled or rippled. This perhaps could be prevented by diluting the etchant slightly. With 10 μm removed from each surface (wafer reduced from 250 to 230 μm), the uneven etch did not appear to effect the behavior of the detector.

The type of epoxy used for edge passivation of these surface barrier detectors is also very important. The epoxy must cover the area not protected by Ge. Transene epoxy 50 and the CIBA epoxy (mentioned in Appendix A) are designed to have a high resistivity to prevent ohmic leakage. They are of low viscosity to reduce the chance of an air bubble touching the silicon surface (another source of leakage current (REF 3)). These are also "amine type" epoxies, which prevent a conductive surface inversion layer from forming underneath them in the silicon. England recommends passivating the edges with epoxy before evaporating Ge. It was found that this was not necessary as long as the evaporated films were kept away

FIGURE 3.3

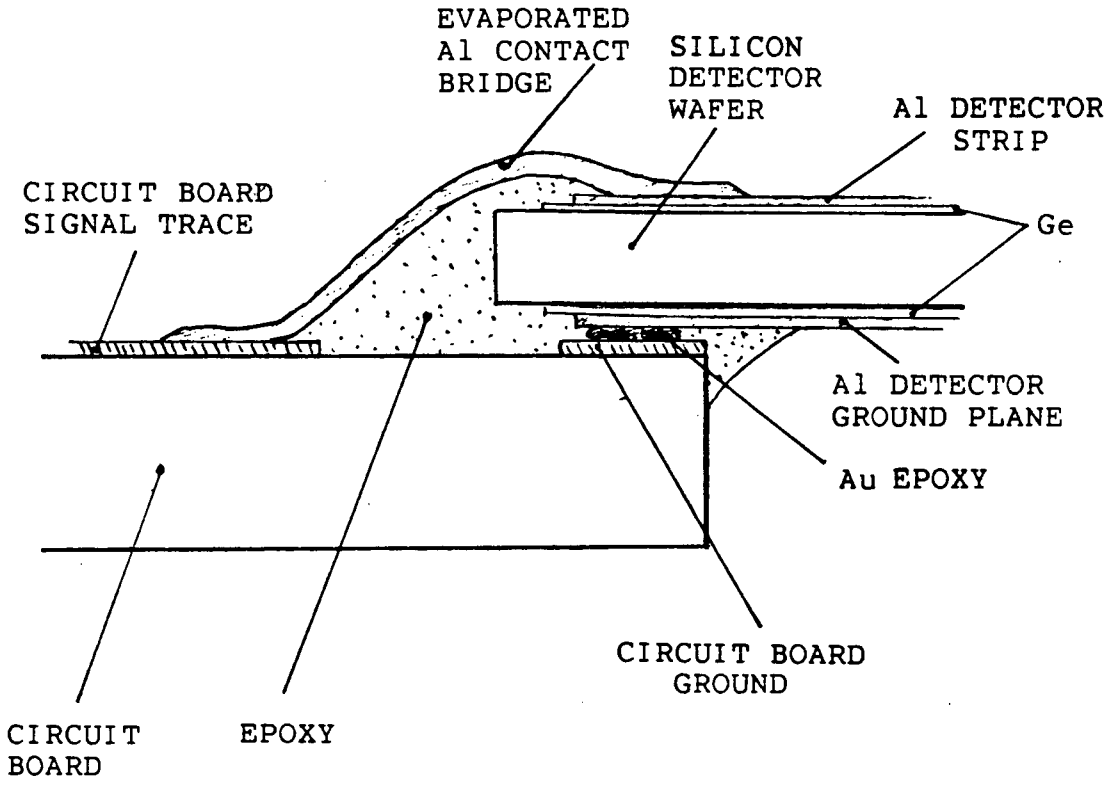

Cross section of the detector circuit board mount and edge passivation.

from the wafer edges (Figure 3.2).

The process developed at UBC uses a second Al evaporation to make contact to the mounting circuit board (Figure 3.3). It is possible, as recommended by England, to do both the contact evaporation and the strip evaporation through a single shadow mask. Care must be taken, however, to avoid electrically shorting strips together if the shadow mask cannot touch the wafer with the epoxy ramp in the way. Ultrasonic wirebonding (used extensively in the semiconductor industry) is another technique available to make electrical contact to the wafer. Wirebonding tends to be time consuming, fragile and may damage the thin film structure of a surface barrier detector, and so is not recommended.

Preliminary electrical characteristics of surface barrier detectors

Before mounting the completed detector wafers, the leakage current and the resistance between strips was measured to assess the quality of the devices.

The resistance between strips on the detector must be much greater than the input impedance of the preamplifiers to prevent crosstalk. Capacitive coupling can also lead to crosstalk but is not so easily measured or controlled. The sheet resistance of the germanium layer is high enough that the resistance between strips was measured at between 40 KΩ and 100 KΩ. This is more than adequate strip isolation.

To measure leakage current, a multipoint probe was used to apply a bias voltage to three adjacent strips. The current flowing in the middle strip could then be measured in a situation similar to the operating configuration. The detectors produced with the modified England recipe had a typical current voltage (I/V) behavior pictured in Figure 3.5. The 1 μA leakage per strip at -30 V was seen to be acceptable as the wafer was expected to be totally depleted at this voltage. The I/V behavior was quite consistent across the wafer with only one or two strips being more than 50% above the average. It was later found that these high leakage strips were more noisy than the rest in the detector that was tested.

One of the surprising results of the I/V measurements in the lab was the asymmetry of the detector. In theory, the symmetric manufacturing techniques should produce a detector that can be biased with a voltage of either polarity. When a negative voltage is applied to the patterned or front side of the detector, the front surface barrier junction is reverse biased and the depletion zone grows from the front toward the back. The electric field in this negative biased detector causes positive current pulses to be seen on the detector strips when particles are detected. Similarly, a positive biased detector will have the back junction reverse biased while the front is forward biased; the detector current pulses will now be negative. Symmetry in the leakage current was expected but not observed. A negative bias proved to give a lower leakage current. This asymmetry can only be caused by

FIGURE 3.4

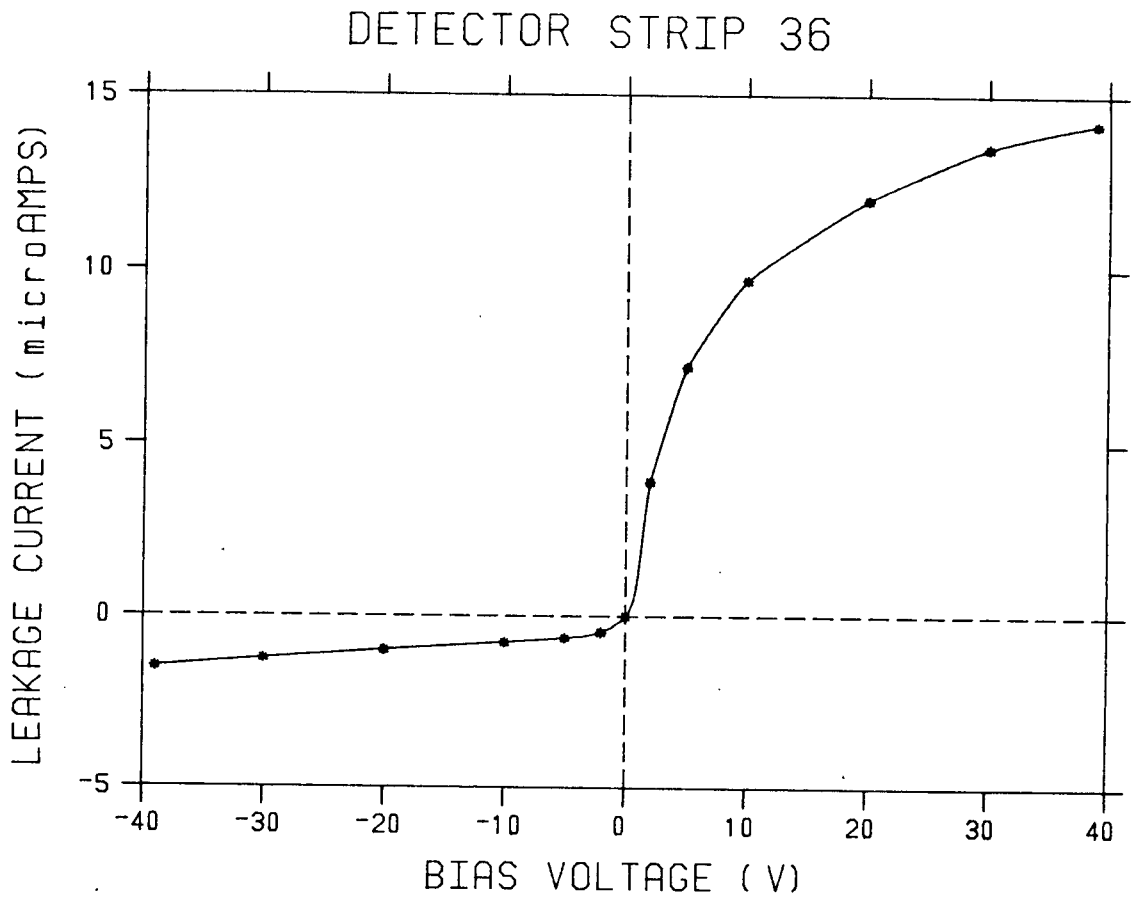

Leakage current of one strip (1mmX30mm) in the SS detector. Negative voltage reverse biases the patterned side of the detector.

the different geometry of the aluminum layers (front is patterned, back is not), as all other qualities of the surfaces are identical. After the wafers were mounted in epoxy, the asymmetry was reduced to a factor of 3, indicating that edge effects are partially responsible. Even more puzzling is that an asymmetry was also seen in charge collection in the finished detector. This charge asymmetry will be further discussed in Chapter IV. Current voltage characteristics show that this type of surface barrier detector is not symmetric as expected.

All solid state detectors act to some extent like a photodetector. The England surface barrier detector is mostly shielded from photons by the aluminum and germanium layers. There is, however, an increase of about 3 $\mu A/cm^2$ leakage current seen when the device is operated in daylight. This increase is roughly constant at all non-zero bias voltages.

Preliminary tests showed that the detector wafers manufactured with the modified England process were acceptable and ready for charged particle tests.

CHAPTER IV

SOLID STATE DETECTOR SYSTEM TEST

A detector amplifier system was assembled using the surface barrier detectors manufactured at UBC. Pion beam tests were performed on the system to measure the efficiency for detecting a transmitted charged particle and the signal-to-noise ratio of the system. The 1 mm resolution was confirmed. Also measured was the charge generation/collection efficiency for alpha and beta particles.

Preamplifier electronics

The preamplifiers used for the prototype system are current sensitive thick film hybrids available from Laben[1] in Italy (part number MSD2). These amplifiers were designed for silicon strip detectors and are high speed (2 ns risetime) with a low input impedance. Particularly useful for strip detectors is their high density (four channels per square inch) and low noise behavior (15 nA RMS equivalent input). The gain was measured at (4±.5) mV/μA in the prototype circuit. For small signals these amplifiers work equally well for positive or negative pulses. In summary, the amplifiers are linear and of lower noise and higher speed than the silicon detector. They are good for observing its behavior, but higher gain would have been useful. A photograph of the

---

[1] Divisione Laben, 20133 Milano, telex 312451

FIGURE 4.1

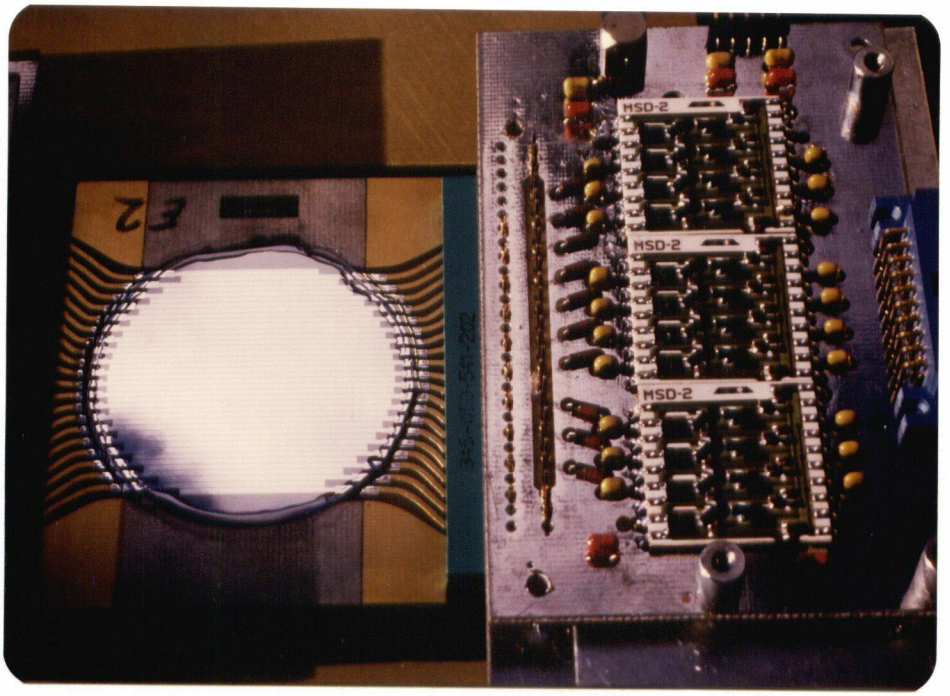

Current sensitive preamplifier array. In spite of the high density Laben hybrids, two layers of circuit boards are used to read out the 20 strips from each side of the detector.

FIGURE 4.2

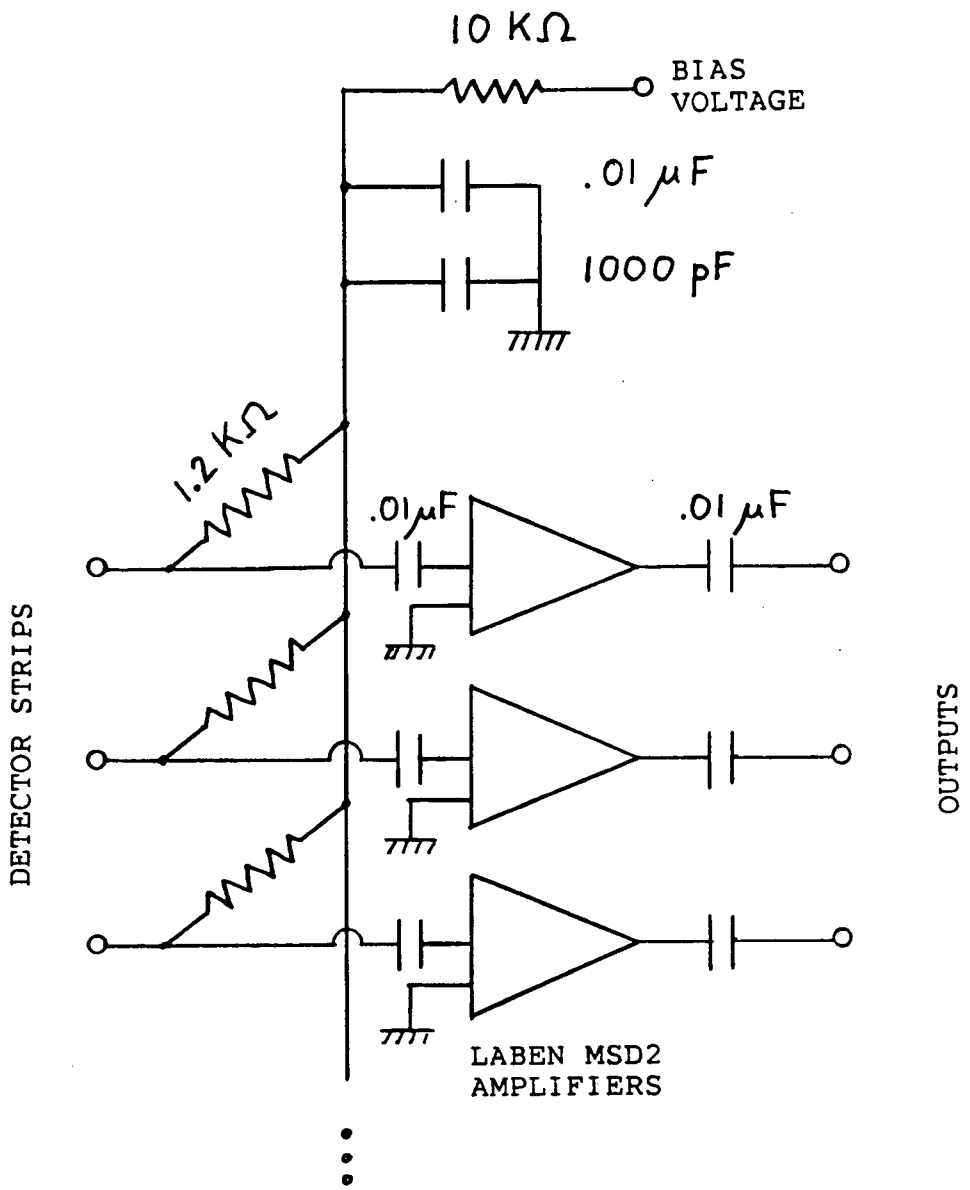

Preamplifier and bias voltage circuit.

detector/preamplifier system is included in Figure 4.1, and a circuit diagram is shown in Figure 4.2.

Alpha source tests, detector asymmetry

Charge collection and generation characterictics of the SS detector were measured with alpha particle signals. A striking asymmetry was observed in charge collection efficiency and time.

Figure 4.3 shows the preamplifier output pulses seen for detected alpha particles from a ^{244}Cm source on the junction side of the detector with several negative bias voltages. The characteristic shortening of pulse width and increase in pulse height can be seen as the bias voltage is increased. The charge collected from the detector is 230 fmC estimated from the area of the voltage pulse and the gain of the preamplifier. The alpha energy is 5.8 MeV; when reduced to 4.8 MeV by losses in 1 cm of air, this gives a value of k=.34 in Equation 2.2 (3.3 eV per electron hole pair). This charge generation efficiency is the same as the 1/3 expected. Uncertainties in these calculations are on the order of 20%. The collection times were seen to be as fast as expected from Equations 2.10; the pulses pictured in Figure 4.3 have rise times on the order of 7 ns. The charge collection behavior of the detector in this configuration is as expected from theory. Crosstalk between adjacent strips and adjacent amplifiers was observed to be less than 20%.

FIGURE 4.3

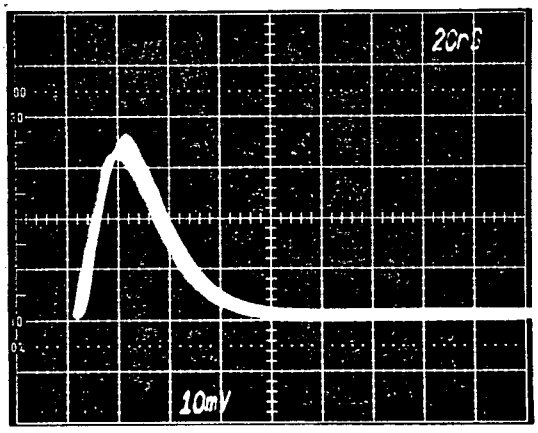

a) BIAS=-19V

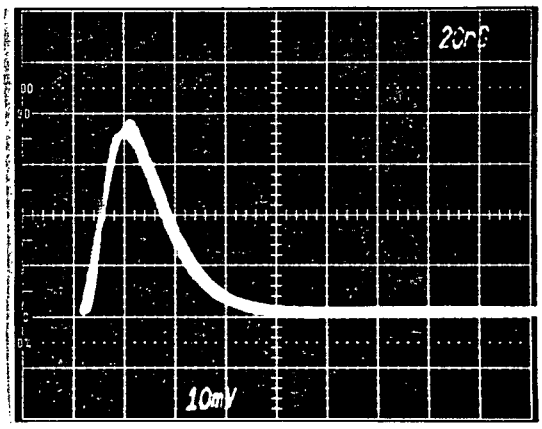

b) BIAS=-25V

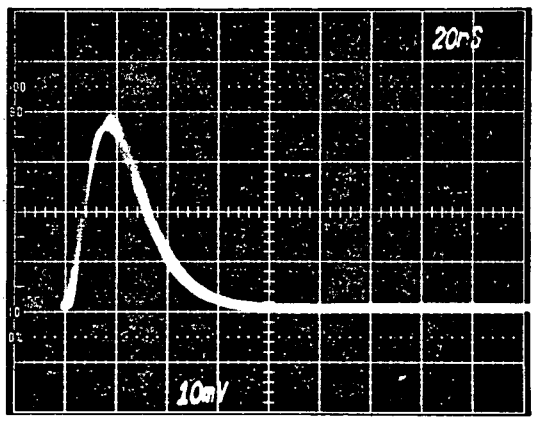

c) BIAS=-32V

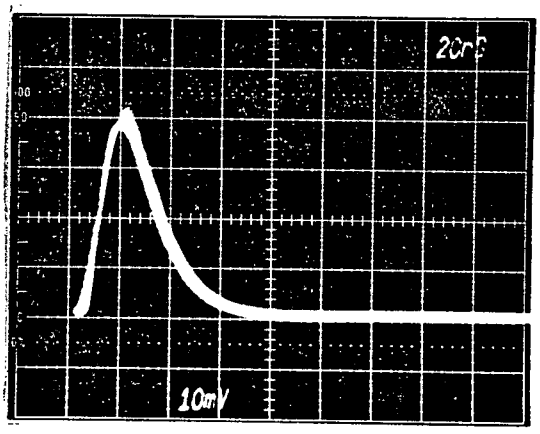

d) BIAS=-39V

Curium 244 alpha pulses for different bias voltages (measured after the preamplifiers). Notice that charge collected (area of pulse) is roughly constant while the pulse height and rise time vary.

FIGURE 4.4

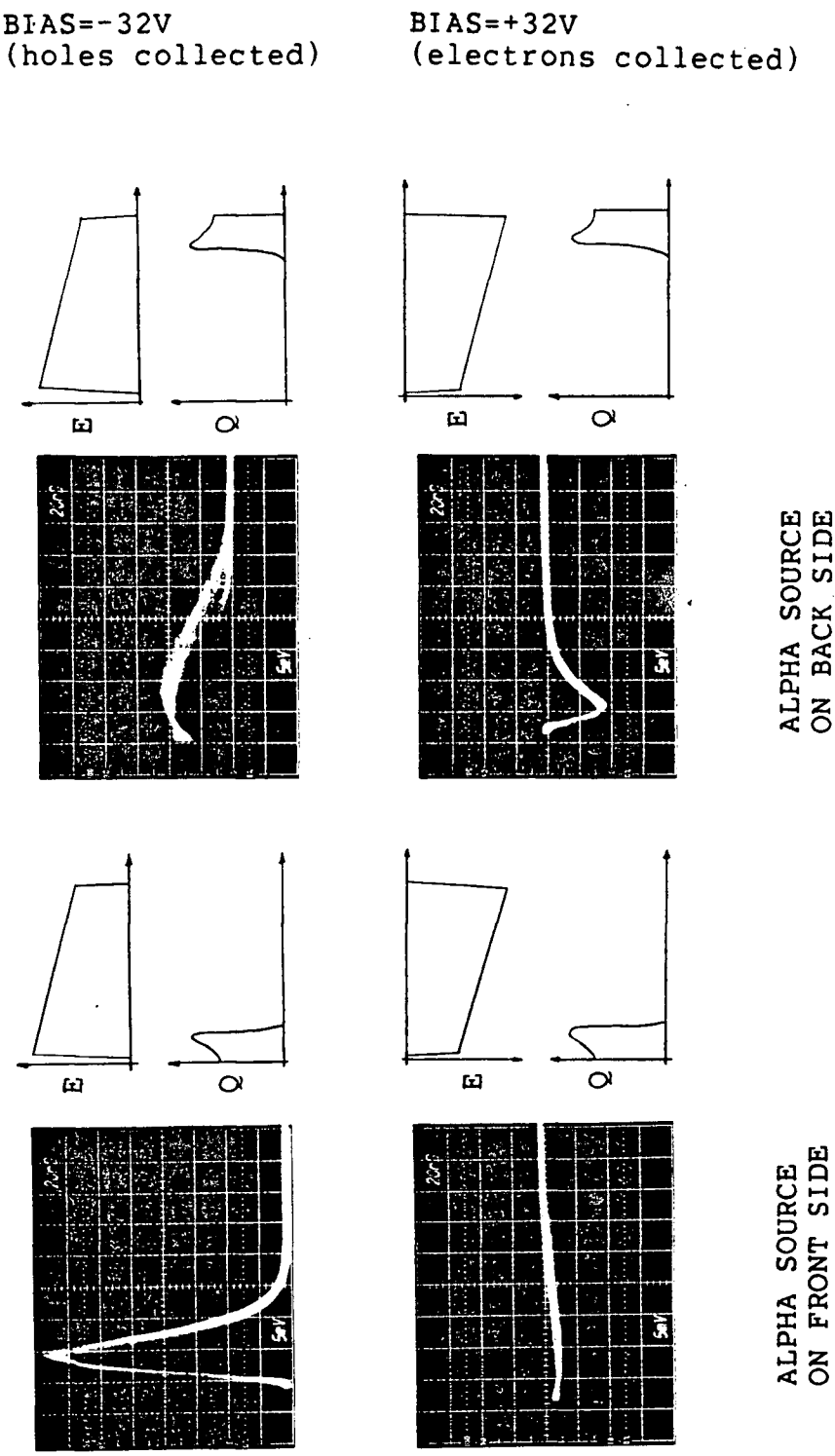

Response of detector to 5.8 MeV alpha particles for different bias polarities and surfaces of entrance for the particles. Sketches of the internal electric field and the initial ionization distribution are included. The left hand side of the sketches represents the front of the detector (patterned side) where the preamplifiers are connected.

When the bias voltage is reversed or the alpha source is placed on the opposite side of the detector from the junction, the behavior changes in a mysterious way. Figure 4.4 shows the pulses observed for the four possible combinations of bias voltage polarity and source position. Also shown are the qualitative electric field and ionization distributions. These observations can be used to estimate the depletion depth of the detector, the charge collection efficiency and the drift time of the charge carriers.

The charge deposited in the depletion zone (≃area of pulse) is seen to be the same for α particles entering either the front or the back of the detector (for a given bias voltage). As the range of the α is at most 28 μm in silicon, this implies that the detector is totally depleted at a bias voltage of ±32 V. The same results were not seen at a bias voltage of ±25 V, indicating that the detector is only slightly over-depleted at 32 V.

The difference in pulse areas seen for different polarities of bias voltage indicates that the charge collection efficiency for holes (negative bias voltage on the front strip side) is three times better than that for electrons. This effect seems to indicate the presence of trapping sites for electrons either in the crystal bulk or in the surface.

The extreme widening of the detector pulse seen when the α particles enter on the non-junction side of the detector is

another unexpected effect. The collection time predicted by Equations 2.10 are at most the order of 20 ns. In addition, the collection times are predicted to be larger for holes than electrons, which is not seen in the data. This pulse time lengthening effect is correlated with the absolute strength of the electric field where the α energy is deposited. The discrepancies from Equations 2.10 can possibly be explained by space charge effects on the local electric field due to the large charge densities generated by α particles.

Beta source tests

β particles from a ^{106}Ru source were used to observe the detector response to small signal transmitted particles. ^{106}Ru decays to ^{106}Rh which in turn β decays with a peak energy of 3.5 MeV. The peak energy lost by the β particle in 230 μm of silicon is about 250 KeV when particles from the low end of the energy spectrum are almost stopped by the detector. Photographs of the detector response to β particles are shown in Figure 4.5. The pulses are about 30 ns long and show no evidence of the lengthening observed for α particle pulses. The 1/3 charge reduction effect is still seen, however, when the bias voltage is switched from negative to positive. As a result of the charge collection asymmetry of the prototype, the electronics for further tests were designed to receive positive pulses from a negative biased detector.

FIGURE 4.5

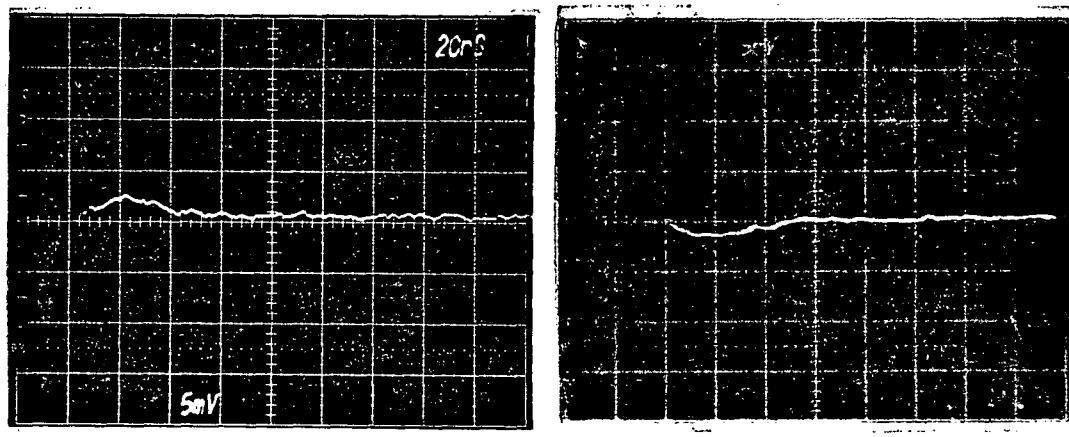

BIAS=-32V

BIAS=+32V

20ns per division
5mV per division

Detector pulses seen (after preamplifiers) for beta particles from a Ruthenium 106 source.

FIGURE 4.6

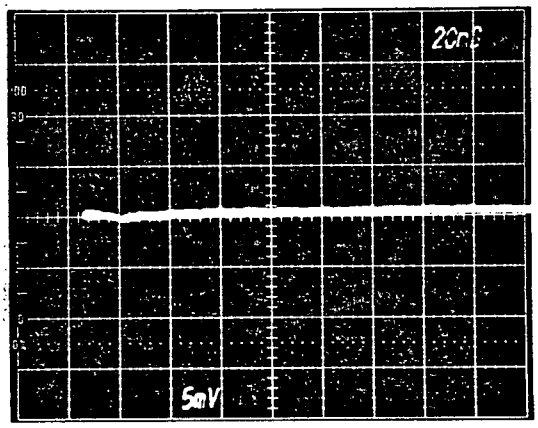

BIAS=0V

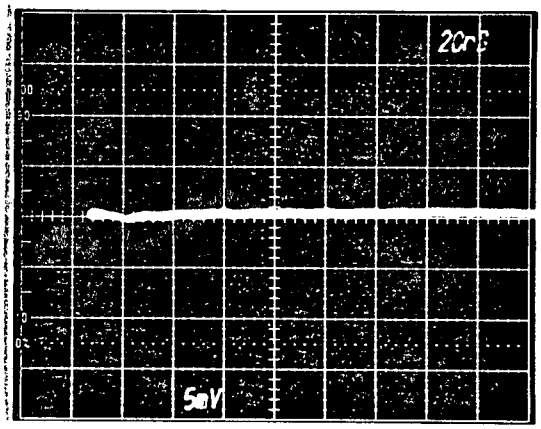

BIAS=-39V

5mV/div
20ns/div

Noise seen at output of preamplifiers.

Observed noise of system

The noise seen on an oscilliscope in the output of the preamplifier was about 1 mV peak to peak (.2 μA RMS equivalent input to preamplifier)(Figure 4.6). What is interesting is that this noise did not change with bias voltage on the detector or with exposure of the detector to daylight. The noise appeared to be mostly caused by the preamplifiers (in spite of the specifications), as it was only slightly reduced when the detector was removed. This low noise behavior could only be achieved when a battery was used for the detector bias voltage, as power supplies proved to be a significant source of noise.

Beam test design

The prototype detector was tested in the M13 pion beamline at TRIUMF. The efficiency for detecting particles was measured for different particle types and energies at different settings of detector bias voltage. Estimates were also made of the noise level of the system. It was not possible to measure the high rate performance of the detector as the beam flux was too low during the experimental time. Only one wafer was tested extensively.

The detector system was linked to the CAMAC data acquisition system as shown in Figure 4.7. The signals from the preamplifiers on the 40 detector strips were discriminated individually by three LeCroy 2735A units. The logical ECL

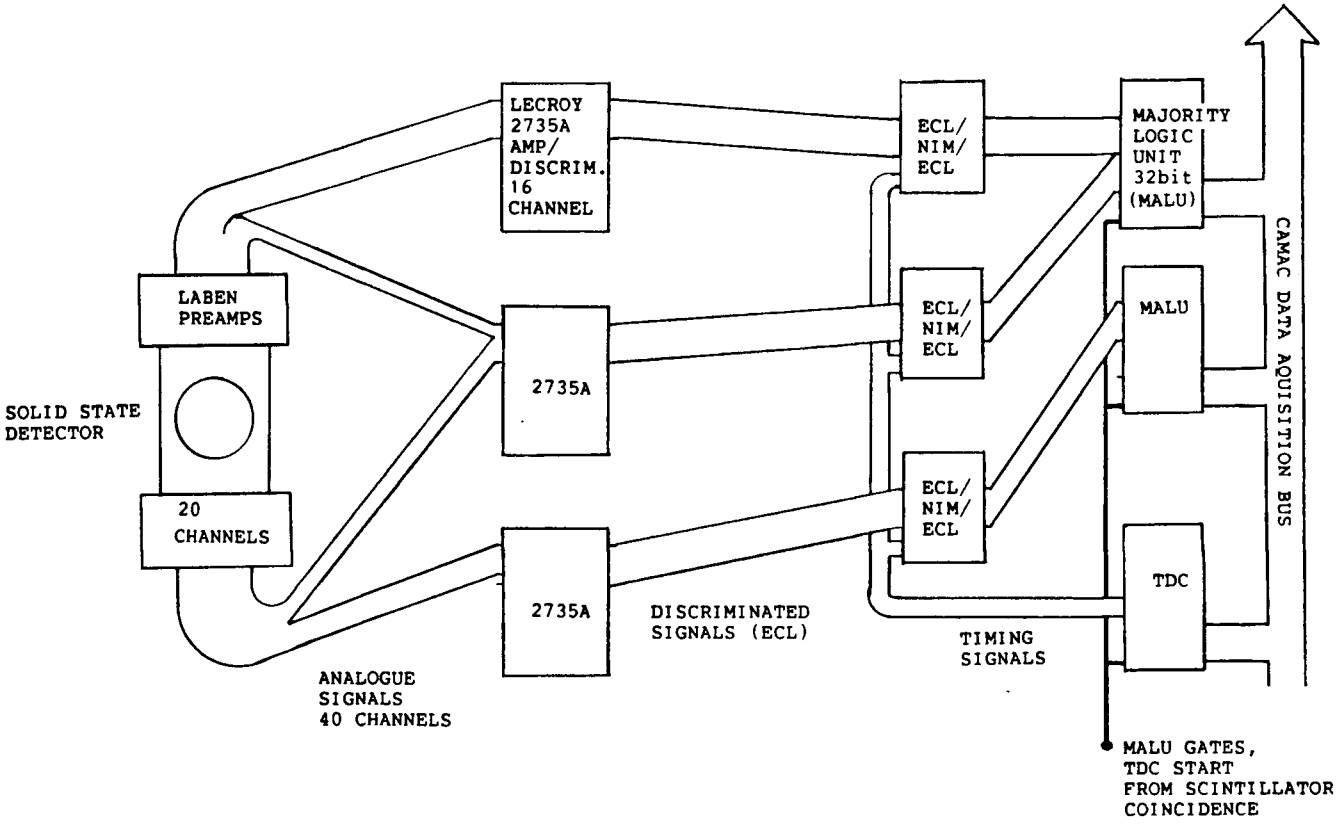

FIGURE 4.7

Block diagram of detector data aquisition electronics for the pion beam test.

output pulses from the 2735A's were read in the counting room by CAMAC majority logic units. The 2735A amplifier discriminators do not give an analogue signal output so the size of the signal pulses could not be recorded directly.

In addition to the strip detector, two delay-line multi-wire proportional chambers were used for ray tracing and two scintillators were used for a trigger (Figure 4.8). The delay line chambers had a resolution of 1 mm in the vertical or Y direction and 2 mm in the X direction. The strip detector was oriented to be position sensitive in the Y direction.

The M13 beamline was set at two momentum values during the test. With the channel set at 128 MeV/c (slits open to give 10% $\Delta p/p$ momentum window) the beam is roughly 95% π^+, 3% μ^+ and 2% e^+. Heavier particles are stopped in the first scintillator. The pion energy at this momentum is 50 MeV. With the channel set at 96 MeV/c (30 MeV pions) the fraction of electrons and muons goes up to about 8% each. By using time of flight information, it is possible to distinguish the three particles in each event observed. A range of particles from minimum ionizing up to more than twice minimum ionizing was available for the test. Approximately 30,000 detector events were recorded for each detector configuration.

Beam test, position resolution

Measurement of the SS detector position resolution was performed by ray tracing with the wire chambers. This was done

FIGURE 4.8

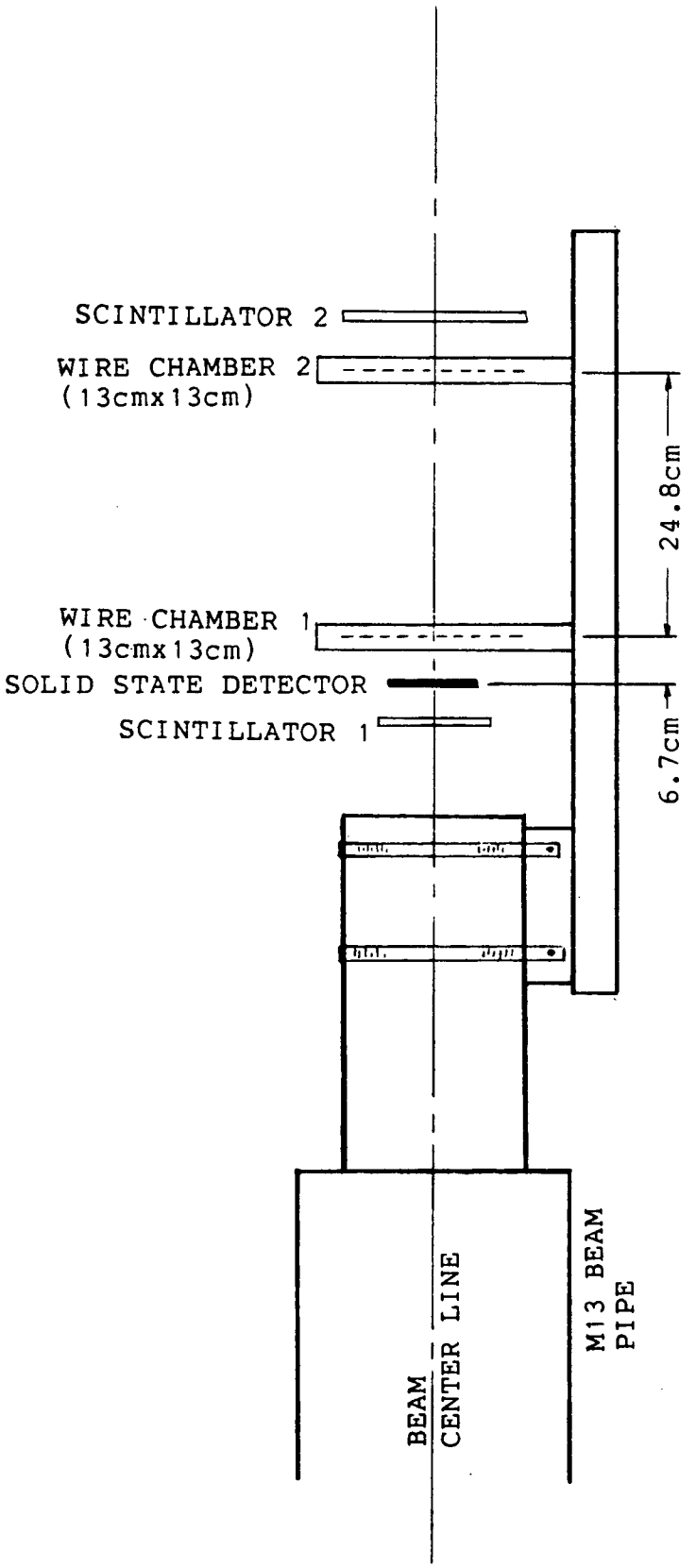

Solid state detector beam test apparatus.

FIGURE 4.9

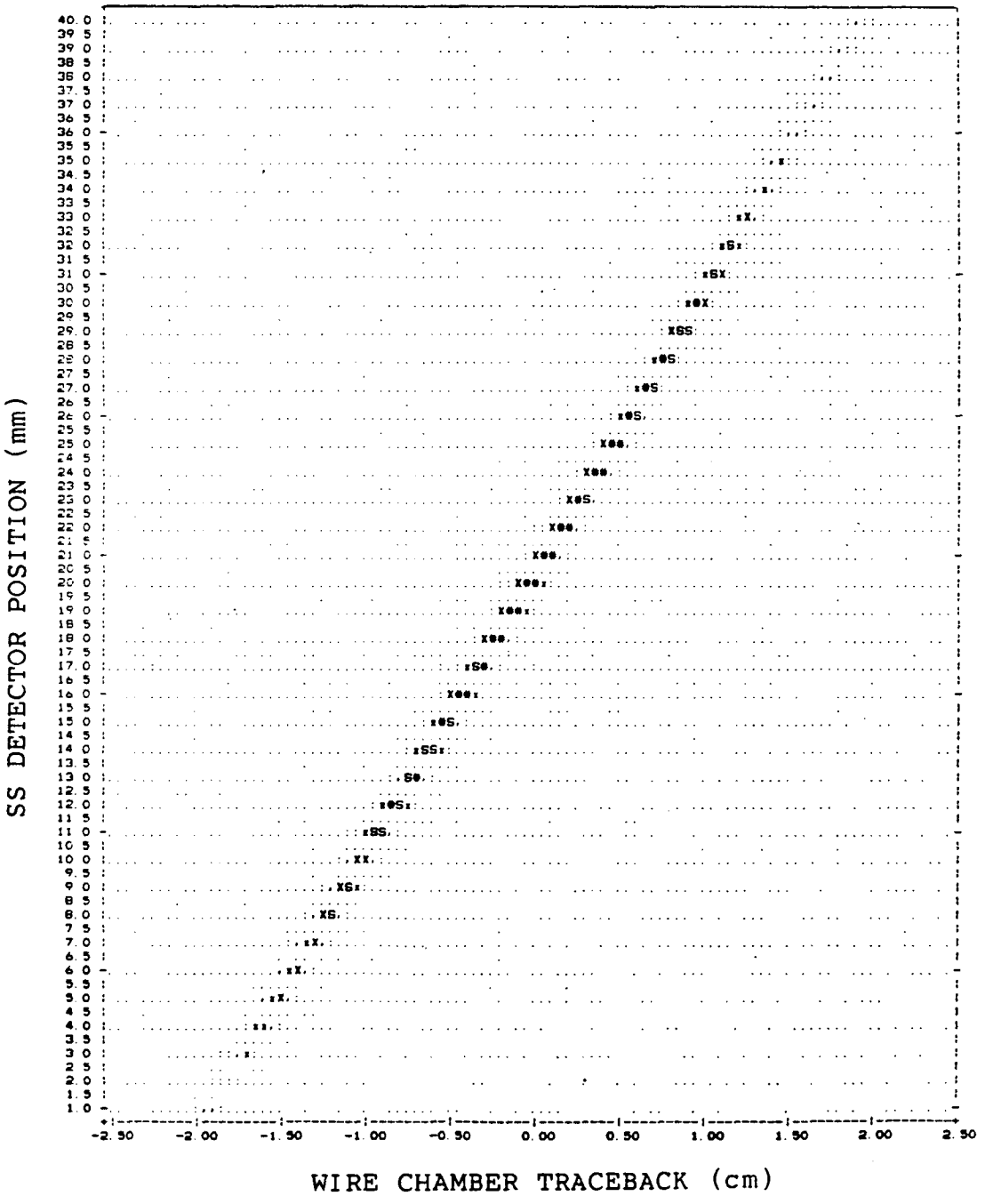

Scatterplot of SS detector position (single or adjacent double hits) versus wire chamber traceback position.

FIGURE 4.10

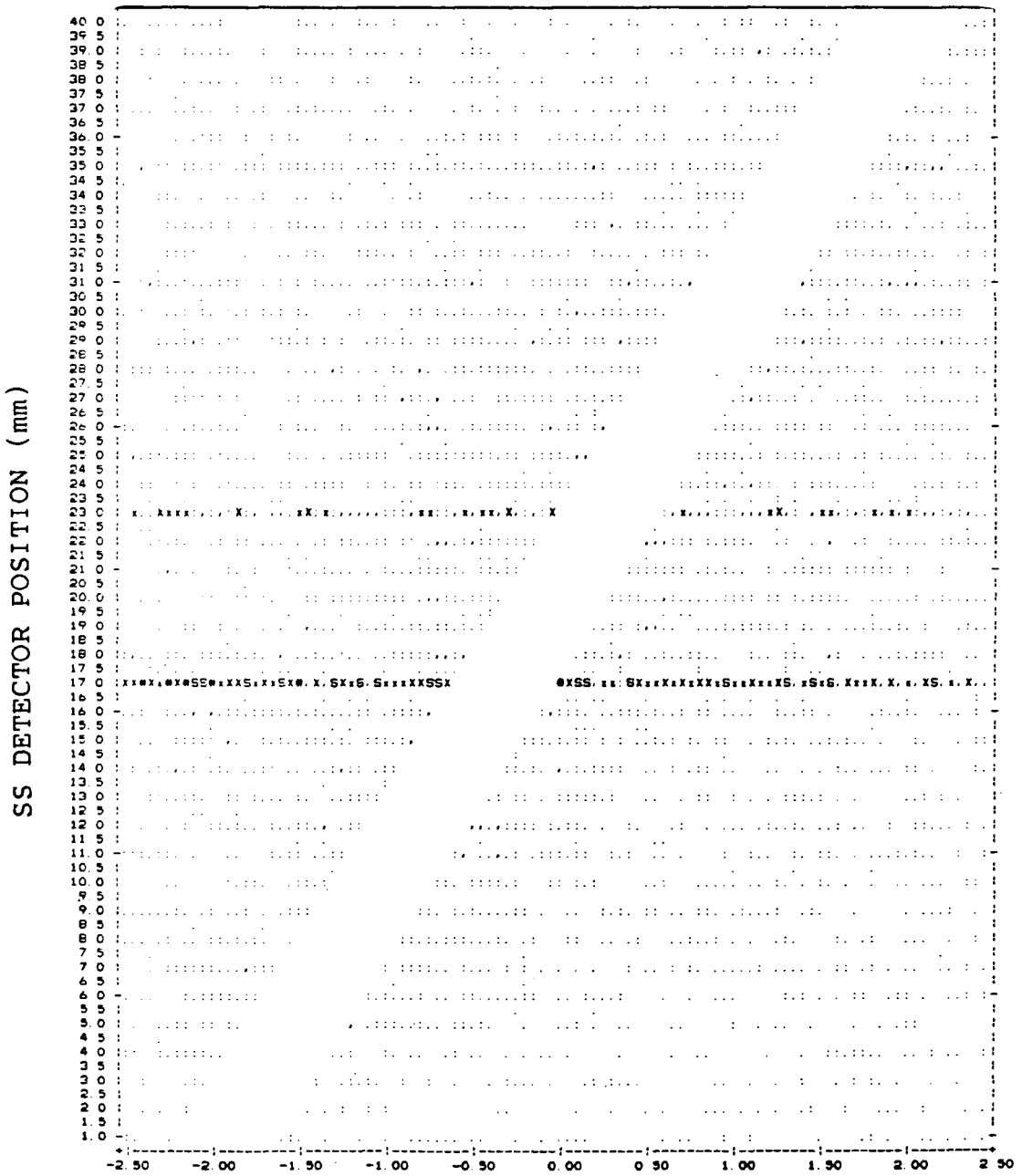

Scatterplot of detector position versus wire chamber traceback with only "noise" included. Note the excess noise on strips 17 and 23.

FIGURE 4.11

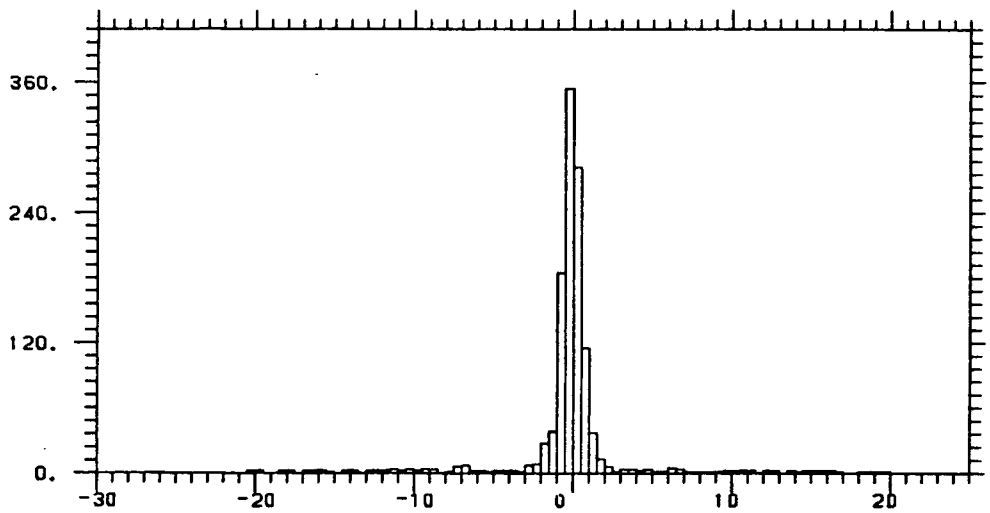

Wire chamber traceback position at detector for hits of strip 20. Note that the resolution of the WC traceback is only 1mm at best.

more to test the total experimental apparatus and to measure noise than to show that 1 mm strips give 1 mm resolution. A scatterplot of wire chamber Y traceback versus detector position is shown in Figure 4.9. Only particles that were traced back through the SS detector were considered for analysis. A slice of this plot, the correlation of strip 20 and traceback position, is shown in Figure 4.11. The 1.5 mm width of the peak in Figure 4.11 is exactly what one expects from the correlation of two 1 mm resolution instruments. The events that do not lie on the scatterplot diagonal (Figure 4.10) were considered as noise.

Beam test, noise and efficiency

The prototype system was found to have a low signal-to-noise ratio. Minimum ionizing particles lose about 90 KeV in the detector. This is a signal of only .16 μA based on a 30 ns pulse width and 3.2 eV per electron hole pair. The preamplifier/detector RMS noise has been measured at approximately .2 μA (Figure 4.5).

Preliminary rejection of noise in the strip detector was accomplished by rejecting all detector events with more than one strip hit unless it was a pair of adjacent strips that fired. A typical beam profile as measured by the SS detector is shown in Figure 4.12. Half integer bins represent events where adjacent strips fired. Real double events were ruled out as the beam flux was too low (1 KHz); only at fluxes over 1 MHz is pileup a non-negligible problem. This multiple hit

FIGURE 4.12

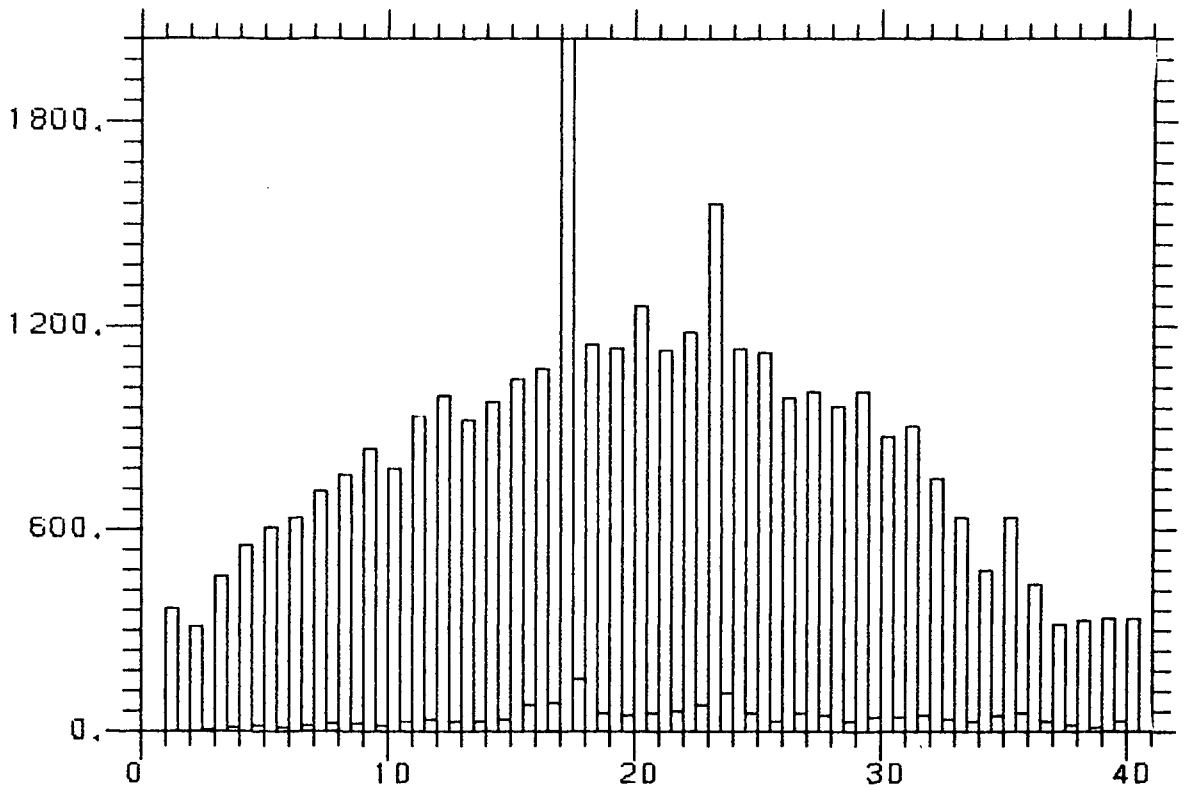

Beam profile as seen with the solid state detector.
Half integer bins represent adjacent double strip hits.

noise rejection system will identify a percentage of noise signals equal to the probability of a real particle being detected. Only when no particle passes through the detector or when a real particle pulse is not discriminated can a noise signal be interpreted as a real event. The largest effect of the noisy system was to reduce the peak efficiency of the detector at low discriminator thresholds. The number of strips fired per particle is shown in Figure 4.13; events in bin zero represent particles that were traced back through the detector but were not discriminated. Figure 4.14 shows the detector efficiency and noise versus discriminator threshold with no noise rejection and with the rejection method described above. Efficiency is defined as the number of particles detected by the SS detector divided by the number traced back through it. The noise is defined as detector events that do not coincide with the wire chamber traceback (Figure 4.10). Strips 17 and 23 show an excessive amount of noise.

The residual noise seen after multiple hit noise rejection is mostly due to pion decay to muons in the test apparatus. The π^+ lifetime, τ, is 2.6 X 10^{-8} s. The fraction, f, of pions that decay in a short distance x is

$$f \simeq x/\beta c \gamma \tau$$

Equation 4.1

where β, γ, are the relativistic parameters associated with the pion in the lab frame. For 50 MeV pions, 4.2% will decay in the 30 cms between the strip detector and the final wire

FIGURE 4.13

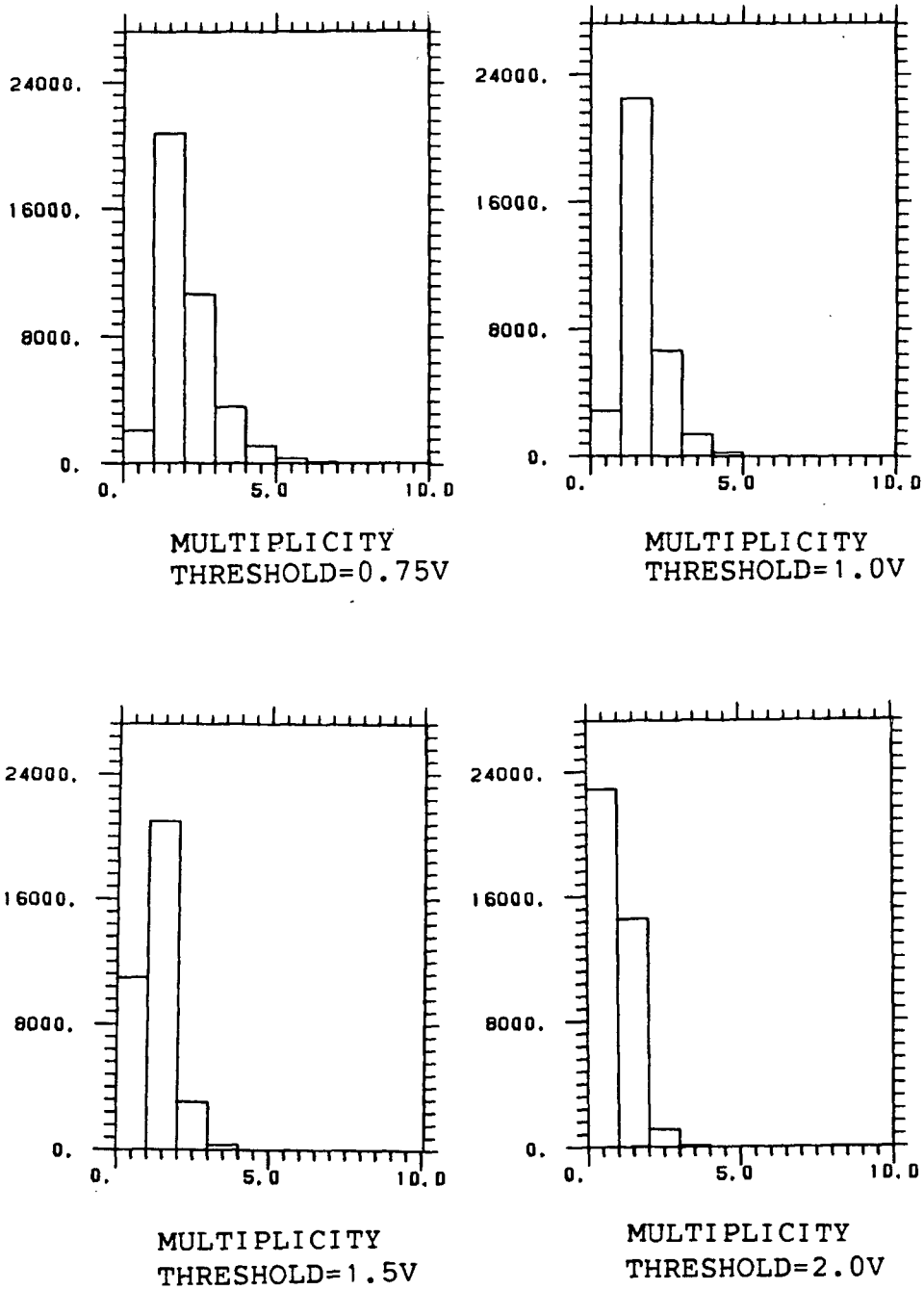

Multiplicity (number of strips fired per event) for different discriminator thresholds. Only singles and some doubles are kept as good events.

FIGURE 4.14

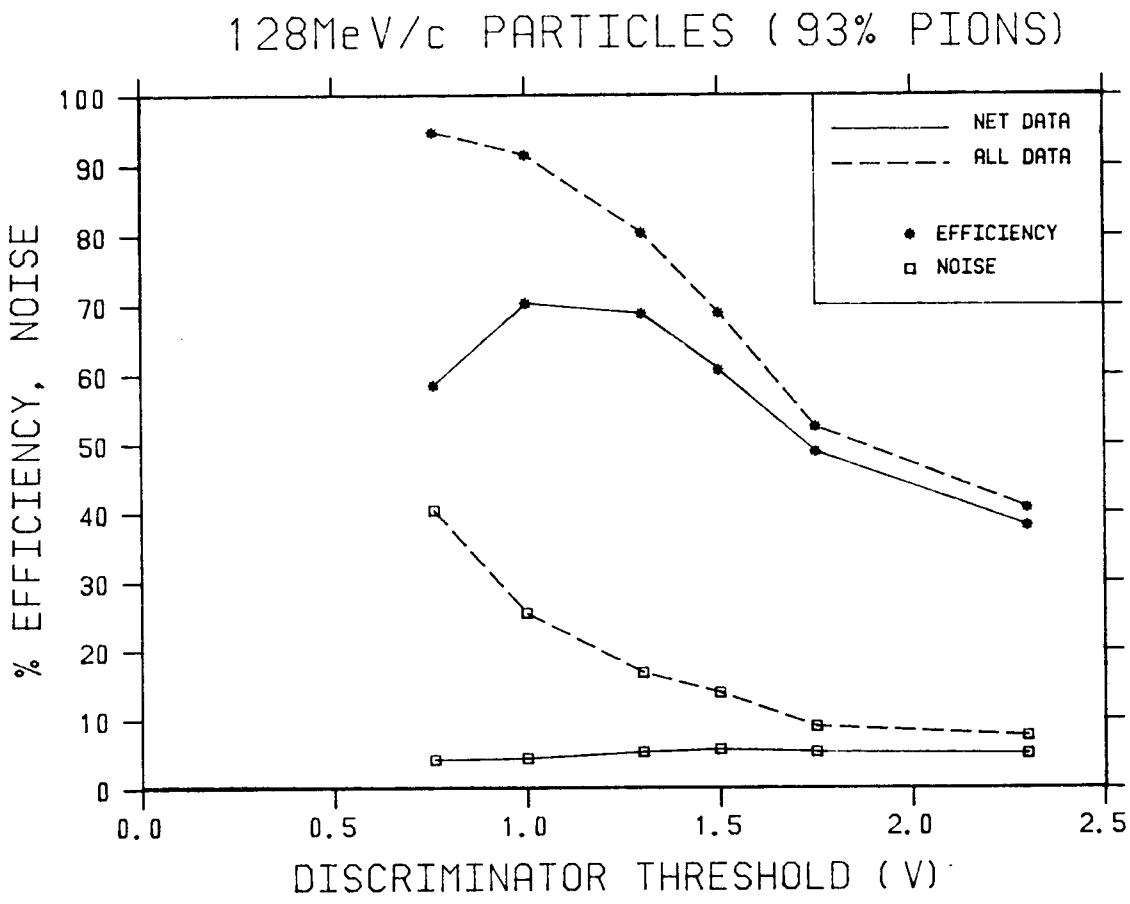

Detector efficiency and noise for a -32V bias voltage. Net data includes only single or adjacent double SS detector hits.

FIGURE 4.15

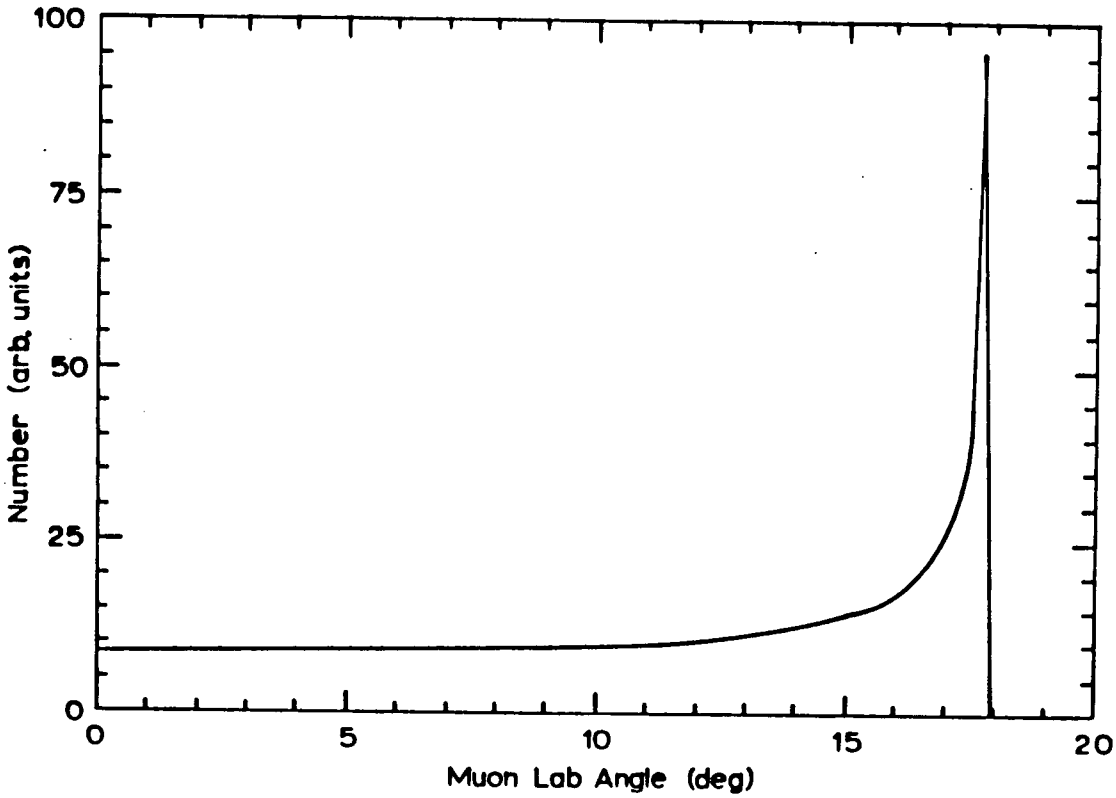

Distribution of lab angle of muons from decay of 50MeV pions.

FIGURE 4.16

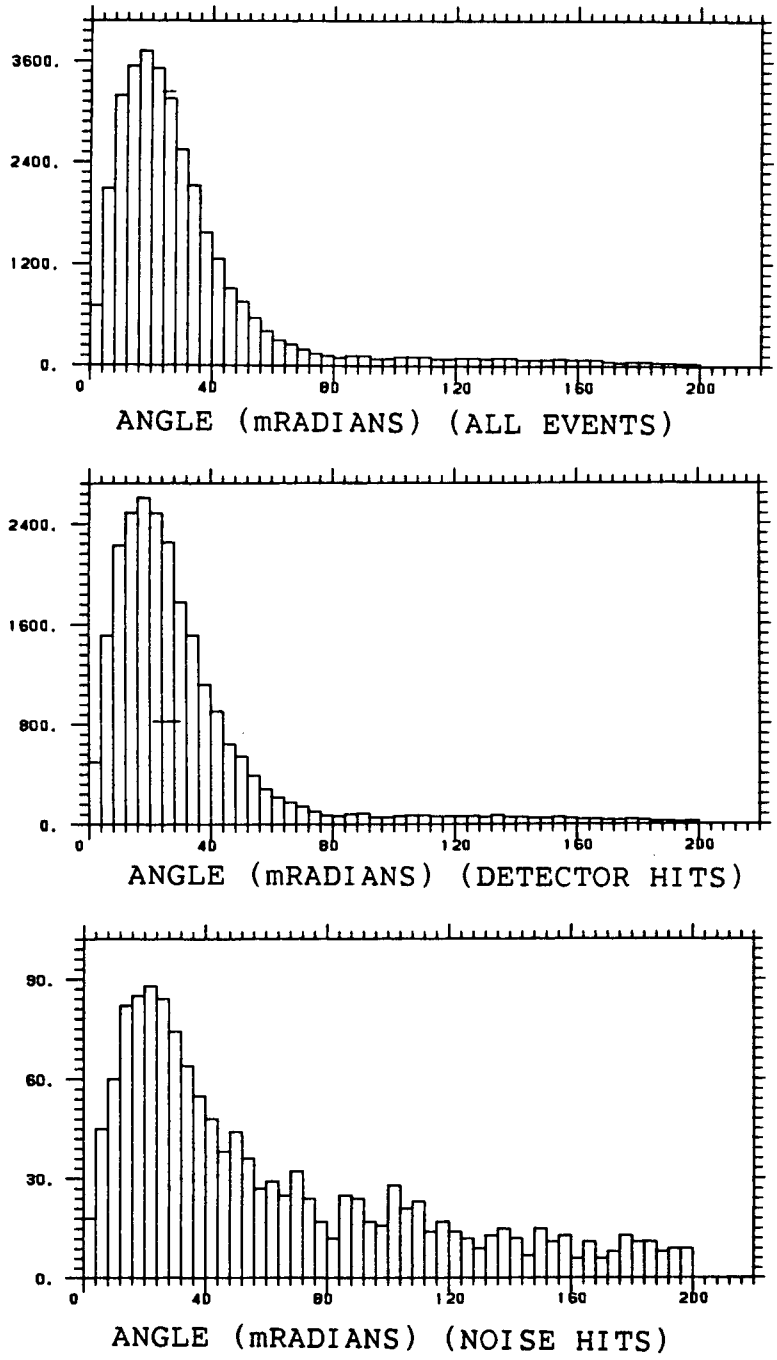

Angle of particle ray through apparatus (beam centre line is defined as zero). Notice correlation between noise signals and angle; this correlation is caused by pion to muon decay in the aparatus.

chamber. the distribution of the resulting muon angle is shown in Figure 4.15 (REF 11). The product muons are detected in the wire chambers but due to the non-zero angle to the original pion path, an erroneous traceback is calculated in most cases. A 3-4% traceback "noise" is expected in the pion test data due to π to μ decay in the test apparatus. Figure 4.16 shows the correlation between angle of traceback path and noise. This correlation supports the π to μ noise hypothesis.

Beam test, bias voltage and efficiency

The efficiency of the detector was measured at three different bias voltages. A summary of the results is represented graphically in Figures 4.17. Unfortunately, only negative biases could be used due to the fixed input polarity of the 2735A discriminators. As was expected, the efficiency for detection improves with increased particle energy loss. The efficiency also increases with increased bias voltage. In the range tested, the detector is of little use for detecting minimum ionizing electrons (less than 50% efficient, large amount of noise) and only of marginal use for the 50 MeV pions it was designed for (70% efficient, low net noise). A further increase in bias voltage would not be likely to improve the performance of the detector as this would increase leakage current. Excess noise was detected on strips 17 and 23, and both of these strips were seen to have leakage currents several times the average ($\simeq$10-20 $\mu A/cm^2$).

FIGURE 4.17a

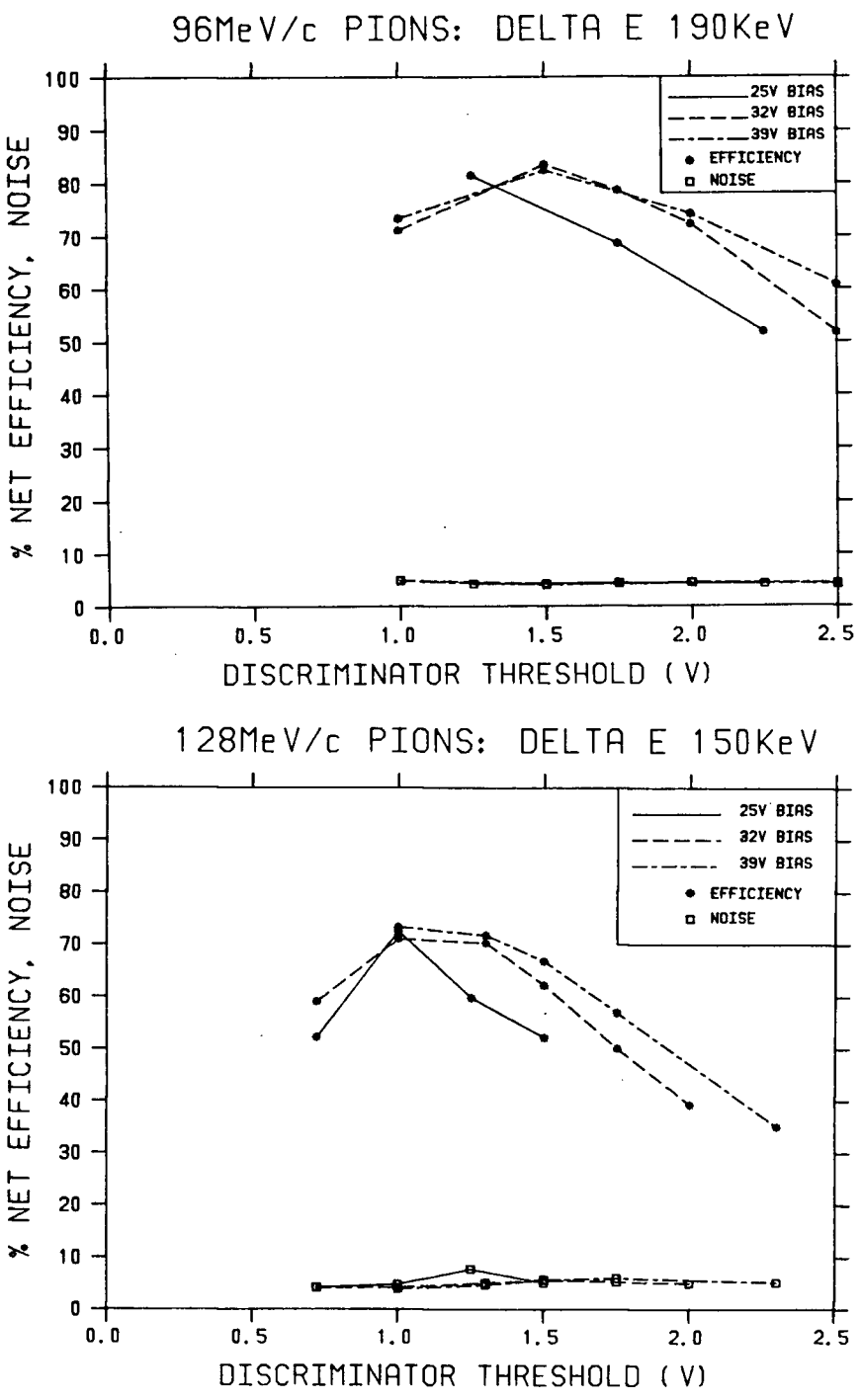

Summary of SS detector efficiencies and noise for various deposited energies, bias voltage and discriminator thresholds. Only single or adjacent double hits are included.
See also figure 4.17b.

FIGURE 4.17b

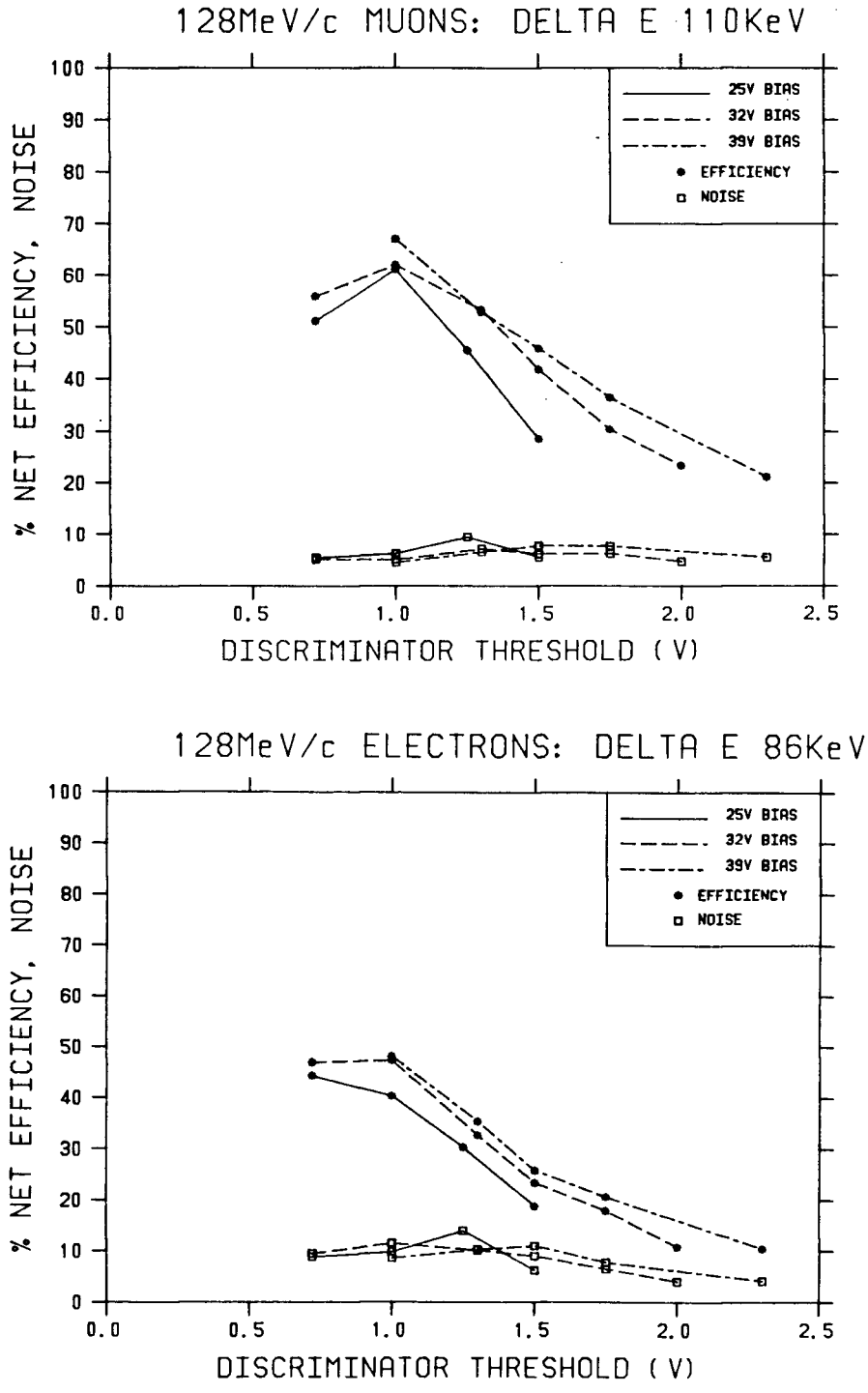

SS detector efficiencies and noise.

Timing of SS detector signals

Timing information for some strips was recorded. Discriminated signals from the strip detector were made available by using an ECL/NIM/ECL converter (Figure 4.7). These signals were recorded in a TDC (time to digital converter) started by the two scintillators. A time spectrum for one strip is shown in Figure 4.18. Even with the primitive time over threshold discrimination, the width of the time peak (time jitter) was only 10 ns. The width of the data acquisition gate to the majority logic unit could then be set at 40 ns, thus reducing random noise.

The time spectrum also showed evidence of RF pickup by the detector. At low discriminator settings, noise peaks separated by 43 ns (characteristic of the cyclotron) could be seen in the time spectrum.

FIGURE 4.18

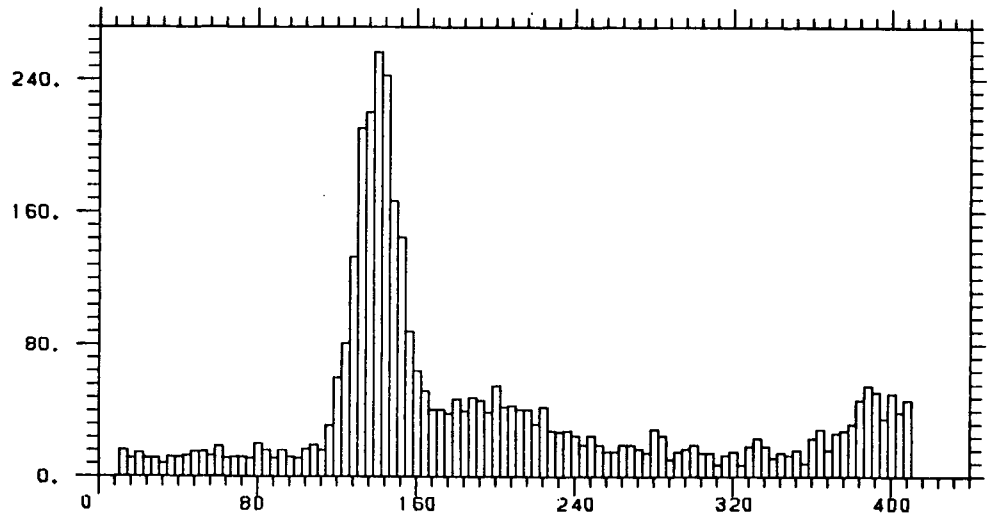

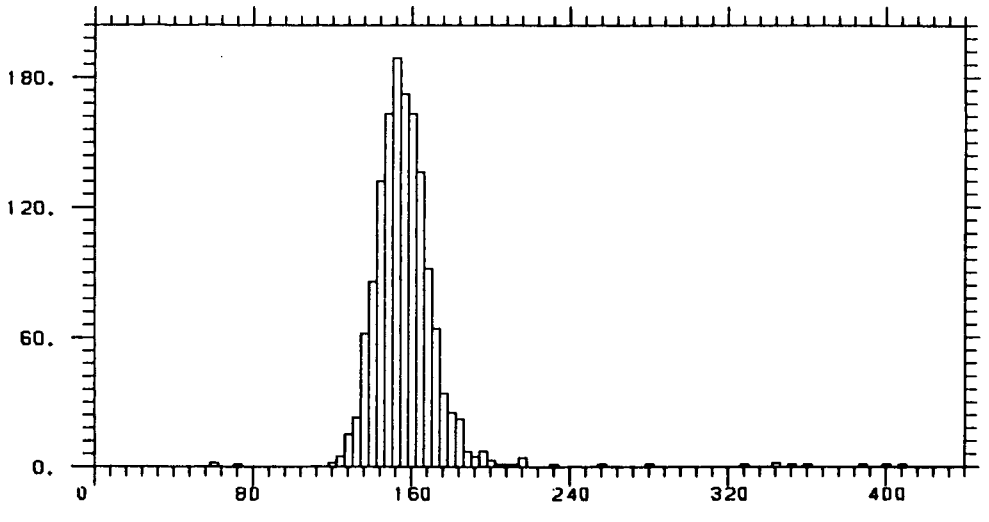

Time spectrum of signals from one strip. At low threshold noise is clearly visible with a component having a 43ns period.

CHAPTER V

SUMMARY AND CONCLUSION

A surface barrier solid state detector system was developed at TRIUMF specifically for position resolution of 50 MeV pions at high fluxes. The efficiency of the prototype detector system was measured at 70% for these particles at low rates. The rate capability of the device is expected to be in excess of 1 MHz per strip as the characteristic signal length was 30 ns. The 1 mm resolution and 40 mm active diameter of the device are adequate for beam profile monitor, active momentum slit, and target position monitor applications in the M13 beamline. The device would be more desireable if postion resolution could be achieved in both directions. The multiple scattering and energy straggle associated with the 55 mg/cm^2 detector is acceptable for the applications proposed although thinner detectors would also be desireable.

Noise, improvements

The low signal to noise ratio and resulting low efficiency of the prototype detector is due to one or more of three sources. There is the intrinsic noise from the detector crystal, RF electro-magnetic pickup, and electronics noise.

Excessive leakage current noise was observed on two strips of the prototype detector. To remedy this problem, more work must be done in the solid state laboratory. All that may

be necessary is the manufacture of several more detector wafers to smooth out problems with cleanliness. As with all fabrication processes, the quality of the product will vary from run to run and the best devices must be chosen for use as detectors.

The strips of the SS detector act as an aerial for ambient RF power. The pickup observed for the unshielded detector was small as the electronics were carefully shielded and grounded. To further reduce this problem, the detector/preamplifier system should operate in a Faraday cage with foil windows, or inside the beam pipe.

Electronics noise appeared to be the biggest problem in the prototype system. On most of the detector strips, application of bias voltage did not increase the noise seen on the output of the preamplifiers. This noise was seen to be the same size as pulse expected from minimum ionizing particles. The LeCroy amplifier discriminators were operated very close to the minimum threshold possible (at which point oscillation occurs), and they may also have contributed a portion of the noise signals. Higher gain low noise combination preamplifier and discriminator hybrids are being considered for the next generation of electronics. These devices, available from Newmarket Microsystems in England, also have an analogue output useful for measuring the energy loss of particles in the detector.

Future considerations

In the immediate future at TRIUMF, development will continue on devices similar to the non-integrated prototype detector. Two dimensional resolution devices are possible, but problems stemming from the asymmetry observed in the prototype device may have to be overcome. Thinner detectors can also be made if the signal to noise ratio is increased.

The next step in the development of position sensitive solid state detectors will be integration of the first stage of amplification on the same wafer as the detector. This will probably be accomplished with GaAs technology. The maximum size of solid state detectors will soon expand to the 8 inch diameter wafers now available.

REFERENCES

1 E.E.Haller, H.W,Kramer, W.A.Higinbothom, Mat.Res.Soc. Vol 16, "Nuclear Radiation Detector Materials", Holland Press

(a) J.H.Howes, J.Watling, P207

(b) A.Musa, J.P.Ponpon, M.Hage-Ali, P225

2 E.M.Lawson, Nuc.Inst.Meth. 180(1981)651

3 J.B.A.England, "Techniques in Nuclear Struture Physics", Part 1, Macmillan Press

4 A.A.Konova, Nuc.Inst.Meth. 160(1979)115

5 J.B.A.England et al, Nuc.Inst.Meth. 196(1982)149

6 J.Kemmer et al, Nuc.Inst.Meth. 205(1983)99

7 W.J.Price, "Nuclear Radiation Detection", second edition, McGraw Hill

8 S.M.Sze, "Physics of Semiconductor Devices", John Wiley and Sons

9 P.Borgeaud et al, "The Effect of Radiation on the Energy Resolution of Ion Implanted Silicon Detectors", Commissariat a l'Energie Atomique Centre d'Etudes Nucleaires de Saclay, France

10 J.B.A.England, V.W.Hammer, Nuc.Inst.Meth. 96(1971)81

11 R. Tacik, Phd Thesis, UBC 1984

12 J.B.A.England, Private communication, Dec 1984

13 J.Yah-Min Lee, IEEE Transactions on Electron Devices, Vol.ED-28,No.4, April 1981

14 P.Janega, Private communication, May 1983

APPENDIX A

MODIFIED ENGLAND PROCESS FOR SURFACE BARRIER DETECTORS

1. Start with high resistivity n^- silicon wafers: polished both sides, $\simeq$ 5000 Ωcm, carrier lifetime $\simeq$3 ms.
2. Clean the slice in solvent (2-Propanol, Acetone) and then in distilled deionized water with ultrasound. (All wet chemicals and utensils must be very clean, all water should be distilled deionized).
3. Boil the slice gently in concentrated nitric acid for 5 minutes. Dilute and decant with distilled deionized water.
4. Boil in water for 5 minutes, dilute and decant with cold water.
5. Etch the wafer in room temperature CP4A (40% HF: concentrated acetic acid: concentrated nitric acid/3:3:5). The wafer must be constantly agitated and tends to form a "rippled" surface anyway. CP4A etches at about 20 μm/min (per side). At least 10 μm should be removed. Quench the wafer in H_2O. Dilute and decant with water (50% dilution, 5 times).
6. Oxidize the wafer in 1% potassium dicromate solution. Place it in the cold solution and heat to 80 C, wait 10 minutes, dilute and decant. At this point, if contamination can be observed as streaks under an infra-red lamp, one may want to start over.
7. Dry the slice in N_2 and place in evaporator.
8. Evaporate 560-750 $\mathring{A}$ of Germanium (p doped semiconductor

grade Ge was used with a starting pressure of 10^{-6} Torr) onto both sides of the silicon, the diode is now formed and passivated by the Ge.

9. Evaporate 210 Å Au or 1100 Å Al onto both surfaces. Strip patterns are made on one surface with a wire shadow mask in contact with the wafer (start at 10^{-6} Torr pressure).
10. Glue the ground plane to the circuit board mounting surface with conducting epoxy (Epotek H44). Make an epoxy "ramp" with Transene epoxy 50 (or CIBA AY105:HY956, 6:1 by weight) and evaporate contacts to the circuit board through a shadow mask (Figure 3.3). The traces on the circuit board should be gold. Often the evaporated contact traces must be probed with a pencil point to make a good electrical contact if aluminum is used for the metal evaporations. The aluminum strips form an insulating oxide layer very quickly in air.